CONTRAST MEDIA & MOLECULAR IMAGING

Received: 11 October 2014, Revised: 30 January 2015, Accepted: 6 February 2015, Published online in Wiley Online Library: 16 April 2015

(wileyonlinelibrary.com) DOI: 10.1002/cmmi.1638

Superparamagnetic iron oxide nanoparticles for *in vivo* molecular and cellular imaging

Shahriar Sharifi[a†], Hajar Seyednejad[b†], Sophie Laurent[c,d*], Fatemeh Atyabi[e], Amir Ata Saei[e,f] and Morteza Mahmoudi[e,g,h*]

In the last decade, the biomedical applications of nanoparticles (NPs) (e.g. cell tracking, biosensing, magnetic resonance imaging (MRI), targeted drug delivery, and tissue engineering) have been increasingly developed. Among the various NP types, superparamagnetic iron oxide NPs (SPIONs) have attracted considerable attention for early detection of diseases due to their specific physicochemical properties and their molecular imaging capabilities. A comprehensive review is presented on the recent advances in the development of *in vitro* and *in vivo* SPION applications for molecular imaging, along with opportunities and challenges. Copyright © 2015 John Wiley & Sons, Ltd.

Keywords: cellular imaging; iron oxide; molecular imaging; MRI; SPIONs; superparamagnetic nanoparticles

1. INTRODUCTION

In the last two decades, molecular/cellular imaging has shown promise for diagnostic and clinical applications (1–3) by allowing for noninvasive visualization of biological phenomena in living subjects. To achieve this purpose, molecular imaging (MI) has combined multidisciplinary expertise and knowledge from several disciplines, including imaging technology, molecular biology, chemistry, medical physics, mathematics, and bioinformatics. The main objective of MI is studying the biochemical processes of diseases without disturbing the integrity of the living subjects, which is usually referred to as noninvasive imaging. Tracking specific biomolecules *in vivo* can highlight the main mechanisms involved in a particular disease. Therefore, the development of new, innovative imaging probes with enhanced sensitivity for the molecular recognition of specific target molecules is an important research frontier (4–8). Different types of imaging technique have inherent advantages and disadvantages (4). There are many modalities suited to MI (see Table 1 for details). Nuclear medicine techniques such as positron emission tomography (PET) or single-photon emission computed tomography (SPECT) are well suited for MI owing to their excellent sensitivity. Using these techniques, vector molecules such as monoclonal antibodies and small molecules labeled with γ-rays or positron-emitting nuclei can be used to monitor receptor engagement with nanomolar resolution. Multimodal imaging, for example PET, combined with computed tomography (CT) helps to superimpose the imaging information from PET with the anatomical information from CT.

Among the various approaches, magnetic resonance imaging (MRI) has many advantages as a diagnostic imaging modality. MRI is not only noninvasive with excellent (submillimeter) spatial resolution, but, unlike PET and CT, it also avoids the use of harmful radiation. Furthermore, MRI yields anatomical information with acceptable soft tissue contrast (8). Perhaps the only unmet challenge with MRI is its relatively low sensitivity, which has led scientists to search for better MRI probes (9).

Almost all MI methods depend on the availability of suitable, highly sensitive reporter systems capable of visualizing submicromolar concentrations of the molecular targets expressed by the tissue or the cell while also discriminating the target signal

* *Correspondence to: M. Mahmoudi and S. Laurent, Nanotechnology Research Center and Department of Nanotechnology, Faculty of Pharmacy, Tehran University of Medical Sciences, Tehran, Iran. E-mail: sophie.laurent@umons.ac.be; mahmoudi@stanford.edu*

† *These authors contributed equally.*

a *S. Sharifi*
Department of Biomaterials Science and Technology, University of Twente, The Netherlands

b *H. Seyednejad*
Department of Bioengineering, Rice University, Houston, TX, 77005, USA

c *S. Laurent*
Department of General, Organic, and Biomedical Chemistry, NMR and Molecular Imaging Laboratory, University of Mons, Avenue Maistriau 19, B-7000, Mons, Belgium

d *S. Laurent*
CMMI – Center for Microscopy and Molecular Imaging, Rue Adrienne Bolland 8, B-6041, Gosselies, Belgium

e *F. Atyabi, A. A. Saei, M. Mahmoudi*
Nanotechnology Research Center and Department of Nanotechnology, Faculty of Pharmacy, Tehran University of Medical Sciences, Tehran, Iran

f *A. A. Saei*
Department of Medical Biochemistry and Biophysics, Karolinska Institutet, Stockholm, Sweden

g *M. Mahmoudi*
Division of Cardiovascular Medicine, Department of Medicine, Stanford University School of Medicine, Stanford, CA, USA

h *M. Mahmoudi*
Cardiovascular Institute, Department of Medicine, Stanford University School of Medicine, Stanford, CA, USA

Biographies

Dr Shahriar Sharifi was born on 28 May 1977 in Tehran. In 2000, he received his Bachelor of Science degree in Material Engineering and graduated with honors from Amirkabir University of Technology (Tehran Polytechnic). Following his graduation, he studied Biomedical Engineering at the same university and received his Master of Science in Biomedical Engineering in 2002 and his first PhD degree in 2007 with specialization in the design and development of biodegradable biomaterials and nanocomposites for drug delivery and medical applications. In 2009, he moved to the University of Groningen, and later on to University of Twente, The Netherlands, where he earned his second PhD, in Medical Science. His current research involves development of smart materials including nanomaterials for biomedical and tissue engineering applications.

Dr Hajar Seyednejad received her PhD in 2012 from Utrecht University (The Netherlands) under the supervision of Dr Hennink and Dr Dhert. She specialized in development of synthetic, biodegradable, and biocompatible scaffolds based on functionalized polyesters for tissue engineering applications. In May 2012, she joined the group of Dr Mikos at the Department of Bioengineering at Rice University (Houston, TX, USA) as a postdoctoral research fellow. During her fellowship, she worked on development of gradient constructs for tissue engineering, using rapid prototyping techniques. Her current research involves development of novel medical devices for biomedical applications.

Dr Sophie Laurent was born in 1967. Her studies were performed at the University of Mons-Hainaut (Belgium), where she received her PhD in Chemistry in 1993. She then joined Professor R. N. Muller's team and was involved in the development (synthesis and physicochemical characterization) of paramagnetic Gd complexes and superparamagnetic iron oxide nanoparticles as contrast agents for MRI. She is currently working on the vectorization of contrast agents for molecular imaging. She is associate professor and co-author of around 200 publications and more than 250 communications in international meetings.

Fatemeh Atyabi is a full professor of pharmaceutics and nanomedicine at Tehran University of Medical Sciences. She is a member of the Controlled Release Society (USA) and the Controlled Release Society of Iran. Dr Atyabi received her PhD degree in Pharmaceutics from the University of Manchester in the UK. Her research fields are in oral drug delivery systems, nanotechnology-based drug delivery systems, especially for anticancer drugs, and tissue engineering. She is the co-author of two book chapters and 120 papers. She is head of the Department of Pharmaceutical Nanotechnology and Biomaterials.

Amir Ata Saei received his PharmD degree from Tabriz University. After working as a researcher in the BioSPION Laboratory in the Nanotechnology Research Center of Tehran University, in 2014 he joined the Department of Medical Biochemistry and Biophysics in Karolinska Institutet to pursue his PhD studies. He is interested in the biomedical applications of nanoparticles and cancer therapy. His previous research was ON gene and plasmid delivery to different cells using nanoscale particles. He is currently focused on anticancer drug target deconvolution and optimizing anticancer therapies by comparative proteomic profiling.

Morteza Mahmoudi received his PhD from the Institute for Nanoscience and Nanotechnology at Sharif University of Technology with specialization in the biomedical applications of superparamagnetic iron oxide nanoparticles. He is Director of NanoBio Interaction Laboratory at Tehran University of Medical Sciences (http://www.biospion.com). His current research involves intelligent control of the protein corona decoration at the surface of nanoparticles and exploring the hidden parameters at the nano–bio interfaces.

Table 1. Imaging modalities employed in molecular imaging and system of detection

Molecular imaging modalities	Means of detection
Computed tomography (CT)	X-rays
Single-photon emission computed tomography (SPECT)	γ-rays
Positron emission tomography (PET)	positrons
Magnetic resonance imaging (MRI)	radiofrequency waves
Optical imaging (OI)	near-IR light
Ultrasound (US)	ultrasound

from the nonspecific background. Among the different MI modalities, nuclear and optical imaging display the highest sensitivity, followed by MRI, ultrasound and finally X-rays (10).

In this review, we intend to focus on MRI based on the application of superparamagnetic iron oxide NPs (SPIONs) as probes (11). In the diverse list of traditional contrast agents, SPIONs provide several advantages, including a relatively low cytotoxicity, high magnetic signal strength, and longer contrast enhancement. The full details of the synthesis procedures for preparation of different types of SPION, together with their corresponding biocompatibility, biosafety, biodistribution, and biodegradation behaviors, are provided in our previous review/research papers (12–19). Therefore, the main theme of this review article is recent advances in the early detection of various human disorders and conditions using SPIONs as MRI contrast agents.

2. SUPERPARAMAGNETIC IRON OXIDE NANOPARTICLES

A number of previously published articles have reviewed the different methods used for preparation of SPIONs of different sizes, shapes, and qualities, together with their diverse biomedical applications (12,20–23). In this section, we will provide a short overview of the characteristics of SPIONs.

Numerous parameters determine the efficiency of SPIONs as MRI contrast agents, such as the size of the iron oxide crystals, the nature of the coating, the hydrodynamic size of the coated NPs, polydispersity, and surface charge. Overall, these characteristics have a significant impact on the colloidal stability, cellular uptake, protein adsorption and interactions with biological membranes, and biokinetic parameters such as biodistribution, biodegradation, metabolism, and elimination (see Fig. 1) (21,24).

The fine synthesis of SPIONs is a relatively complex process: the two main challenges are the monodispersity of the magnetic core and the reproducibility of the synthesis. Various approaches have been followed to produce SPIONs, which include but are not limited to standard iron chloride precipitation, thermal decomposition of organometallic precursors, hydrothermal synthesis, microemulsion and sonochemical methods, sol–gel synthesis, and the polyol method (25,26). Each of these techniques has its own pros and cons. For instance, although the co-precipitation method is easy and scalable, it produces SPIONs with a large size distribution (27). In contrast, mono-dispersed SPIONs can be produced by thermal decomposition; however, the particles fabricated using this technique have hydrophobic surfaces and need to be further modified for biomedical applications (28).

After the synthesis of the core, which is usually made of magnetite (Fe_3O_4) or maghemite (γ-Fe_2O_3), the surface of the SPION is usually covered with a compatible coating to prevent agglomeration of the colloidal suspension and to enhance biocompatibility (29). Many natural and synthetic polymers have been used as coatings, such as dextran and carboxymethylated dextran (30–35), alginate (36–39), starch (40,41), polyethylene glycol (PEG) (42–47), poly(D,L-lactide-co-glycolide) (PLGA) (48–50), and organosilane (29,51–53). Some small charged molecules such as citrate, amino acids, hydroxamate, and dimercaptosuccinic acid have also been used as SPION coatings (54–57).

Other than colloidal stability, several different attributes must also be fully characterized by different analytical methods (58–60). The size of the crystals is measured by techniques such as transmission electron microscopy (TEM) or X-ray diffraction (XRD), and the hydrodynamic size is obtained by photon correlation spectroscopy (PCS), which is also known as dynamic light scattering (DLS). The charge on the surface of the SPIONs can be measured by the zeta potential, which is based on studying the electrophoretic mobility. Although MR efficiency is characterized by measuring the magnetization and relaxation rate, the superparamagnetism of a SPION is confirmed via magnetometry (25,26,61). The latter method also provides information on the specific magnetization and the mean diameter of the iron oxide crystals. It is now well known that many proteins cover the surface of NPs upon their entrance into biological fluids (62). The type and composition of the associated proteins in the protein corona can change the *in vivo* efficacy, targeting efficiency, and fate of NPs (63,64). There are several methods to evaluate the NP protein corona, including liquid chromatography, mass spectrometry, gel electrophoresis, and differential centrifugal sedimentation (65).

The efficiency of a contrast agent or its relaxivity depends on its ability to accelerate the proton relaxation rate, which is defined as the increase of the relaxation rate of the protons of the solvent (water) induced by 1 mmol L^{-1} of the active ion.

$$R_{i(\mathrm{obs})} = \frac{1}{T_{i(\mathrm{obs})}} = \frac{1}{T_{i(\mathrm{dia})}} + r_i C; \quad i = 1 \text{ or } 2 \qquad (1)$$

In the above formula, $R_{i(\mathrm{obs})}$ and $1/T_{i(\mathrm{obs})}$ are the global relaxation rates in an aqueous system, $T_{i(\mathrm{dia})}$ is the relaxation time of the system before addition of the contrast agent, C is the concentration of the paramagnetic center expressed in mmol L^{-1}, and r_i is the relaxivity (s^{-1} $mmol^{-1}$ L). The magnetic relaxation characteristics can be measured by studying the nuclear magnetic resonance dispersion (NMRD) profile, which finally yields information about the mean crystal size, the specific magnetization, and the Néel relaxation time (66).

MRI using SPIONs helps distinguish pathological tissues from healthy surrounding tissues. The preferential accumulation of SPIONs in one type of tissue enhances the image contrast by decreasing the T_2 MRI signal. Another important consideration in using SPIONs for biomedical applications is to graft them with targeting vector molecules so that they can recognize specific cell types or tissues *in vivo* through active targeting (67,68). Although targeting molecules must theoretically increase the accumulation of SPIONs in the target tissue, a recent line of evidence suggests that the protein corona may cover the targeting ligands and considerably reduce the targeting yield (69,70). In addition, the protein corona affects the relaxivity and MRI contrast efficiency of SPIONs (71). On the other hand, passive targeting is based on the physiological differences between pathological and normal tissues (72) and, in the context of

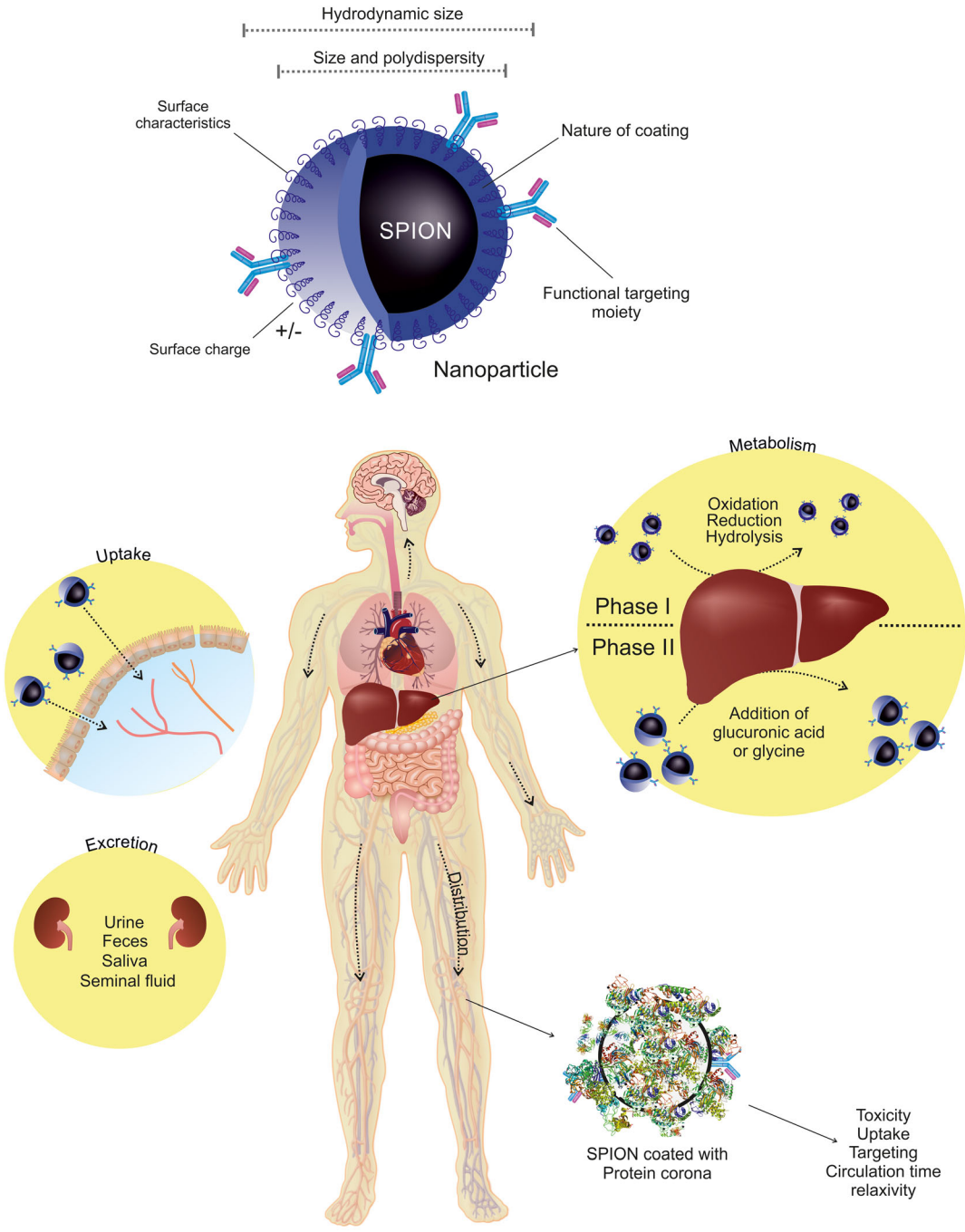

Figure 1. The different physiochemical properties of SPIONs affect their biokinetics and fate *in vivo*. These changes can be observed in uptake, distribution, metabolism, and excretion of SPIONs from body. Protein corona is yet another factor that is influenced by various physiochemical features of NPs and can, in turn, affect the targeting capabilities of SPIONs in imaging applications. Not only can protein corona alter the toxicity, uptake, targeting, and circulation time of SPIONs, but it can also affect the relaxivity of SPIONs as MRI contrast agents.

cancer, mostly relies on the enhanced permeability and retention (EPR) effect of tumor vasculature. However, in passive targeting, NPs might also be taken up by healthy tissues such as cells of the reticuloendothelial system (RES), e.g. those situated in the liver or the spleen (RES organs) (73–75). Therefore, SPIONs can be used for detecting diseases in macrophage-rich tissues (76,77) (see Fig. 1). Upon intravenous injection, NPs are easily and rapidly sequestered by macrophages, resulting in hypointensity of T_2-weighted images. Because tumor tissues are devoid of macrophages in comparison with normal adjacent tissues, tumors can be visualized with increased intensity in MR images (78). One important disadvantage of RES uptake is that the majority of the SPION dose is lost in unspecific tissues.

Under these considerations, three approaches might be followed to prepare molecular probes based on SPIONs: (i) engineering NPs with RES-evading properties, (ii) preserving the bioactivity of targeting molecules through coupling reactions, and (iii) exploiting the protein corona for targeting. In the next sections, we will discuss the strategies for vectorization of SPIONs as well as their applications in specific biomedical disciplines.

3. MOLECULAR IMAGING

NPs are composed of thousands of iron atoms, which provide a large T_2 effect. After coating, chemical grafting is possible via functional groups present on the NP surface or through adsorption. The first strategy used to vectorize NPs was adsorption of antibody (79,80) or protein (81,82) onto the SPION surface; however, this method suffers from difficulty in controlling the reproducibility of the noncovalent grafting as well as the orientation of the targeting moieties. Another strategy is based on streptavidin–biotin chemistry (83–86). Several covalent conjugation strategies have also been developed that involve reactions with amino, carboxylic, aldehyde, or thiol groups (87). Glutaraldehyde bioconjugation (88) and amide formation in the presence of 1-ethyl-3-(3-dimethylaminopropyl)carbodiimide (EDCI) on carboxylated SPIONs have been described for peptide (89–91) and protein (92–94) grafting. Another method is based on the generation of aldehydes on a polysaccharidic coating, such as dextran, through an oxidative conjugation process (95–102). Such oxidative processes have been employed to graft amino-PEG–folic acid onto NPs and to obtain folate-coated pegylated SPIONs (103,104).

Josephson *et al*. (105) have described a method in which the vector molecules can be covalently linked to the SPION surface through a three-step reaction sequence. In this method, a peptide/protein could be attached to the amino group of cross-linked dextran-coated SPIONs via different linkers such as *N*-succinimidyl 3-(2-pyridyldithio)propionate (SPDP) (106–111) (disulfide bond formation), succinimidyl iodoacetate (105,108,112–118) (carbon–thiol formation), activated suberic acid (119–122) (amide formation), succinic anhydride (123) (amide formation), EDCI (87,109,123,124) (amide formation), thionyl chloride (109) (ether formation), or epoxide (109) (carbon–nitrogen bond formation). Utilizing SPDP as a linker has the advantage that the number of reactive amines produced on the SPION can be deduced by spectrophotometric quantification of the pyridine-2-thione, which is released upon reaction with dithiothreitol (DTT). Furthermore, when ligands react with SPDP-functionalized NPs, pyridine-2-thione is released again and can be used to determine the number of conjugated species.

The vectorization of NPs using biomolecules can also be carried out using 2,3-dimercaptosuccinic acid (DMSA) and SPDP (125). Although the particle is coated with DMSA, the vector is linked to SPDP through a peptide bond. These units are subsequently bridged using an S–S linkage between DMSA and SPDP. This coupling methodology has been used to graft antibodies and annexin V to DMSA-coated NPs (55,126–131).

Biomolecular vectors can also be covalently conjugated onto SPIONs previously bound with silane-coupling materials such as 3-aminopropyltrimethoxysilane (APTES) (132) or triethoxysilanepropyl succinic anhydride (TEPSA) (133). Silica coating has been used to conjugate folic acid (104,134) and bovine serum albumin (BSA) (29,135) onto magnetite SPIONs. Initially, the surface of SPIONs is modified with an aminosilane coupling agent, followed by covalent linkage of the amino group of the biovector using glutaraldehyde as a cross-linker. Amine-coated NPs can also be readily modified by ligands containing NHS-modified carboxylic acids or isothiocyanates. Vectors with carboxylic groups can be conjugated to the surface of silica-coated NPs. Carboxylic acid-coated NPs must be initially activated before biological molecules are conjugated. Amine-containing ligands are typically conjugated to carboxylic acid-functionalized particles in the presence of EDCI and sulfo-NHS to yield the corresponding amide.

A 'click chemistry' process based on an azide–alkyne reaction has also been introduced for vectorization of SPIONs with small molecules (136). Click chemistry has shown better efficiency than other methods for conjugation of antibodies to SPIONs. Conjugation reactions based on click chemistry have several advantages over other bioconjugation techniques. Not only does the click reaction take place under relatively mild conditions in aqueous solutions, but also the reaction is simultaneously highly specific, has a high yield, and does not produce unwanted side products. Furthermore, the stable triazole linker resulting from the Cu(I)-catalyzed reaction between the azide and alkyne is biocompatible. In this method, SPIONs can be functionalized with either azide or alkyne moieties by the reaction of carboxylic acid-functionalized NPs with azido-propylamine or propargylamine with EDCI and sulfo-NHS activating reagents in 2-(N-morpholino)ethanesulfonic acid (MES) buffer at pH 6.0. The conjugation reactions have a yield of 90% when conducted at 37 °C for 5–8 h.

In addition, magnetoliposomes have been functionalized with antibodies or peptides (137–143). Nitin *et al*. (144) have functionalized SPIONs with a PEG-modified phospholipid micelle coating. Not only does this coating enhance the water solubility of magnetoliposomes, but the functional moieties of the modified PEG can also accommodate various targeting molecules such as proteins, oligonucleotides, or peptides. For example, multifunctional polymeric micelles composed of NPs and RGD peptides have been recently described for the targeting of cancer cells (145).

In the sections below, the applications of SPIONs and MRI in the imaging of different human conditions as well as stem cell labeling for tracking applications will be discussed in detail. These applications are shown in Fig. 2.

3.1. Inflammation imaging

Upon tissue damage, a cascade of events is launched to repair the injury site. One of the first steps in this process is inflammation, which prepares the ground for tissue healing (146). Due to the involvement of inflammation in the pathogenesis of various human conditions including infection, ischemia, rheumatoid arthritis, atherosclerosis, graft rejection, and the formation of tumor metastasis (146–152), monitoring the inflammatory process is clinically important. Furthermore, misdirected leukocytes may damage healthy tissues by inducing inflammation, and thus molecular methods and markers are required to monitor such processes. For this purpose, target inflammatory cells (e.g. macrophages) can be tagged with SPIONs, usually through internalization of the NPs. Subsequently, SPION-tagged macrophages can invade tissues through inflammatory processes. This methodology has already been applied to a model of inflammation in the central nervous system (CNS) (153,154). For example, upon internalization of SPIONs, microglial cells can be detected by *in vivo* MRI (155,156). However, this application of MRI requires high doses of SPIONs to saturate the macrophages. Such internalization can be observed in SPIONs with opsonin-rich protein coronas (15). SPION-labeled macrophages have also been used for molecular imaging of atherosclerotic plaques (157,158).

Alternatively, specific MR contrast agents could be developed for selective targeting of receptors involved in the inflammatory process (159,160). These markers include cell adhesion

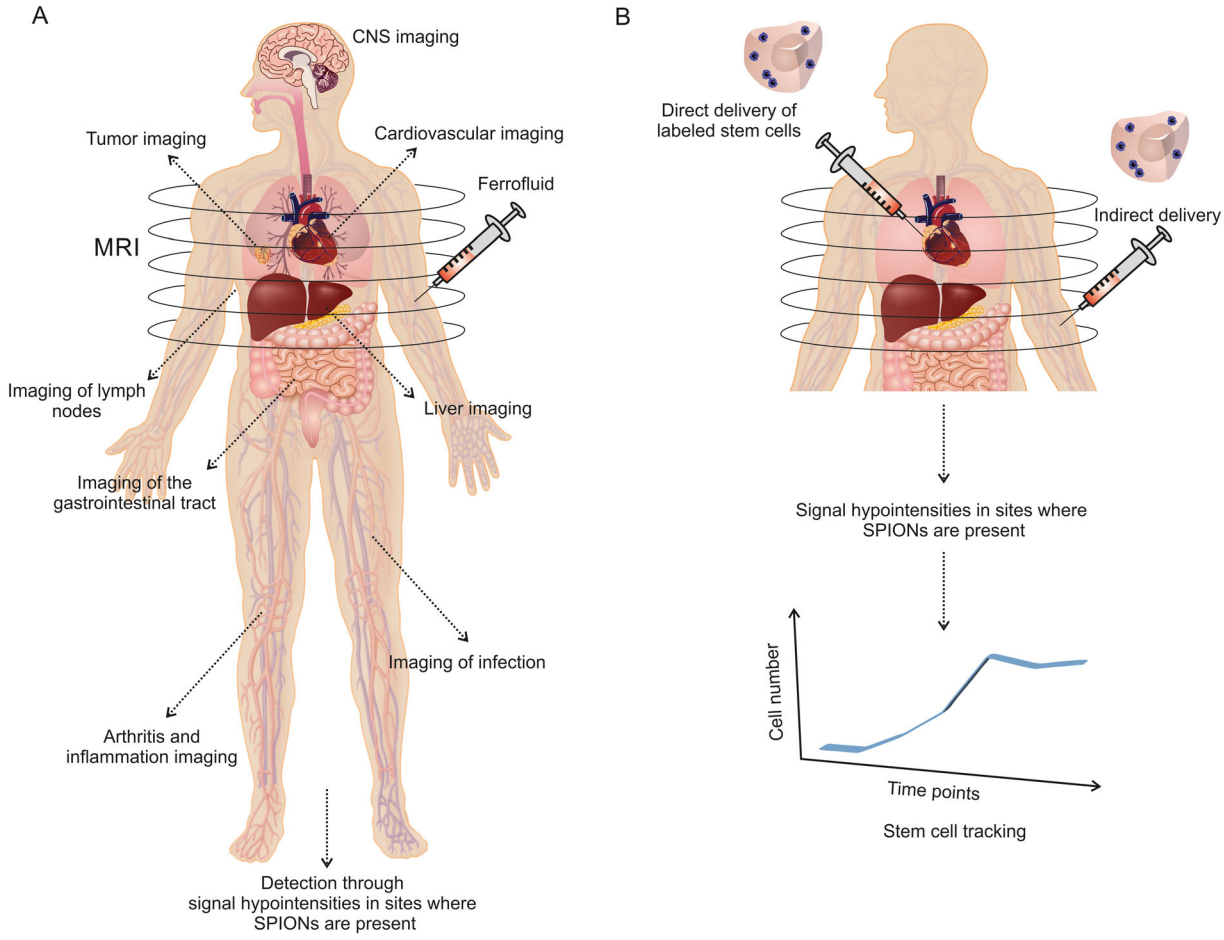

Figure 2. SPION-based MRI has so far had applications in imaging of tumors, CNS, cardiovascular system, gastrointestinal tract, liver, infection, arthritis, inflammation, and lymph nodes. SPION-labeled stem cells can also be used for tracking stem cells after transplantation for monitoring regenerative therapies.

molecules (CAMs), such as E-selectin, which is normally up-regulated in leukocytes and endothelial cells during the inflammatory process (161). A tetrasaccharide, sialyl Lewis^X (sLeX), is the natural ligand for E-selectin (162) and is attached to the leukocyte surface proteins by certain glycosylation enzymes (163). The expression of E-selectin in human endothelial cells has been investigated using cross-linked SPIONs functionalized with anti-human E-selectin antibodies (158). Boutry *et al.* (164) have devised a platform for targeting E-selectin with a mimetic of sLeX that has also been previously used to functionalize other magnetic reporters, such as gadolinium complexes, for the detection of inflammation (149,165–167).

3.2. Molecular tumor imaging

Because nanoparticulate drug delivery systems hold the most promise for the diagnosis and therapy of cancer, many studies have focused on using targeted NPs for *in vitro* and *in vivo* tumor imaging. In tumor targeting and imaging, macromolecular antibodies against cancer cell surface receptors are the most favored targeting moieties for the functionalization of NPs due to their high specificity (168–170). Human epidermal growth factor receptor 2 (Her-2/neu receptor) is a well-known tumor target. Yang *et al.* (171) fabricated poly(amino acid)-coated NPs, to which approximately eight Her-2/neu antibodies were attached per particle. The *in vivo* experience with these NPs revealed by T_2-weighted MRI confirmed that the functionalized NPs could specifically target the Her-2/neu receptors on the cell surface because a significant difference was noted between the NP-treated and untreated cells for the overexpression of Her-2. Song *et al.* used monoclonal antibody fluorescent–magnetic–biotargeting multifunctional nanobioprobes (FMBMNs) to detect and isolate different types of tumor cell, such as leukemia cells or prostate cancer cells (Fig. 3) (172).

Although from a targeting perspective an antibody is an ideal choice for functionalization of NPs, the antibody-targeted NPs suffer from their large hydrodynamic size and diffuse poorly through biological barriers, and this may also lead to easy uptake by RES. Therefore, some studies have also functionalized NPs with single-chain antibody fragments (scFvs) or peptides with smaller molecular weights than full antibodies. As tumor targeting ligands, scFvs have several important advantages over their full antibody counterparts.

Because scFvs are relatively small, they result in the production of smaller NPs, more suitable for crossing biological membranes. Antibodies are more readily internalized by RES organs than smaller scFvs (173,174). Furthermore, unlike antibodies, scFvs do not lose their antigen-binding capacity. Moreover because scFvs lack an Fc constant domain, the chance of immune reactions to these molecules is lower. Last but not least, the production of scFvs is associated with lower costs than that of antibodies.

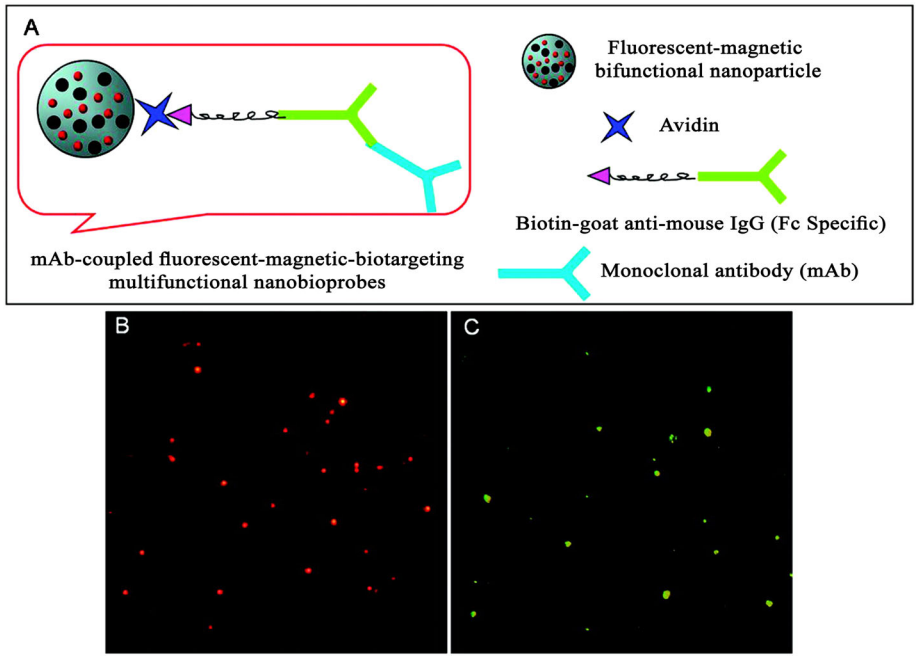

Figure 3. (A) Schematic drawing of an mAb-coupled fluorescent–magnetic–biotargeting multifunctional nanobioprobe (FMBMN). Fluorescent–magnetic bifunctional NPs were covalently coupled with avidin. They were then coated with biotinylated goat antimouse IgG (Fc specific) via the biotin–avidin interaction. Mouse monoclonal antibody (mAb) was then attached to the NPs via the binding to the goat antibody. (B), (C) Fluorescent microscopic images of anti-CD3 mAb-coupled red nanobioprobes (B) and anti-PSMA mAb-coupled yellow nanobioprobes (C). Each fluorescent dot came from a single mAb-coupled FMBMN containing multiple quantum dots. Reproduced with permission from Song *et al.* (172). Copyright (2011) American Chemical Society.

In one study, NPs functionalized with EGFR scFv were shown to specifically bind to EGFR, as evidenced by a decrease in the MRI signal at the tumor site (Fig. 4) (175,176). Although the targeted NPs accumulated selectively within the pancreatic tumors, bare NPs did not produce a distinctive MRI signal in the tumor.

More than 50% of human breast cancers express receptors for luteinizing hormone releasing hormone (LHRH), a decapeptide (177). Leuschner *et al*. (178) prepared NPs conjugated with LHRH, which could selectively accumulate in primary tumor cells and metastatic cells. Because several tumors are also known to overexpress transferrin (Tf) receptors (TfRs), Tf-SPIONs have been used for the specific labeling and detection of gliosarcoma (179–181) and breast carcinoma (95). Furthermore, synaptotagmin 1 protein, which is specific for anionic phospholipids present in apoptotic cells, was used to functionalize SPIONs and thus provided specific contrast enhancement of apoptotic tumor cells treated with chemotherapeutics.

The folate receptor (FR) is generally overexpressed in cancerous tissues. Folate molecules (folic acid, FA) have been grafted on several SPIONs with different coatings such as dextran, PEG, 2-carboxyethyl phosphoric acid, or 2,2′-(ethylenedioxy)bisethylamine. Using FA as a targeting ligand has a number of advantages, such as (i) a high binding affinity for its receptor ($K_d = 10^{-10}$ M) and (ii) a lack of immunogenicity (182). Choi *et al*. (183) published the first *in vivo* study with FA-conjugated dextran-coated NPs, the specific tumor uptake of which was concomitant with a decrease in tumor signal intensity of 38%. Sun *et al*. (184) showed that FR-positive HeLa cells could internalize 1.410 pg iron per cell after incubation with FA-conjugated NPs for 4 h, which was 12 times higher than the uptake of cells cultured with nontargeted NPs. Another similar study on FA-targeted NPs demonstrated the capability of these NPs to selectively accumulate in human nasopharyngeal epidermoid carcinoma cells both *in vitro* and *in vivo*, and to produce appropriate MRI signals (185).

Another overexpressed receptor on the surface of cancer cells is the urokinase plasminogen activator receptor (uPAR). Regarding the fact that the amino-terminal fragment (ATF) of the urokinase plasminogen activator (uPA) can specifically bind to uPAR on the cell surface, Yang *et al*. (175) conjugated this peptide to amphiphilic polymer-coated NPs. They finally showed the selective accumulation of these targeted NPs in the tumor mass in a human pancreatic cancer model. Other similar specific peptides that have been employed for functionalization of NPs in MRIs of pancreatic cancer are cholecystokinin linked (82) and secretin linked (186).

Angiogenesis is a crucial process supporting tumor growth and development by supplying oxygen and nutrients to cancer cells. Because $\alpha_v\beta_3$ l, also known as the cell adhesion molecule integrin, which resides on the surface of tumor vessels, is a marker of angiogenesis, it can be directly targeted. Regarding the fact that the tripeptide arginine-glycine-aspartic acid or the so-called RGD specifically binds to $\alpha_v\beta_3$ (found in tumor vessels) with a high binding affinity, it is usually used to functionalize SPIONs in the targeting and detection of several tumors, including those of breast cancers as well as malignant melanomas and squamous cell carcinomas (187). In a study by Zhang *et al*. (188), after targeting the tumor vessel, RGD–ultrasmall superparamagnetic iron oxide particles (USPIONs) led to changes in T_2 relaxation, and the subsequent signal changes were associated with the $\alpha_v\beta_3$ integrin expression level. In another study, Liu *et al*. (189) demonstrated that HUVECs can internalize RGD-SPIONs, which label $\alpha_v\beta_3$ integrin. In the periphery A549 tumor

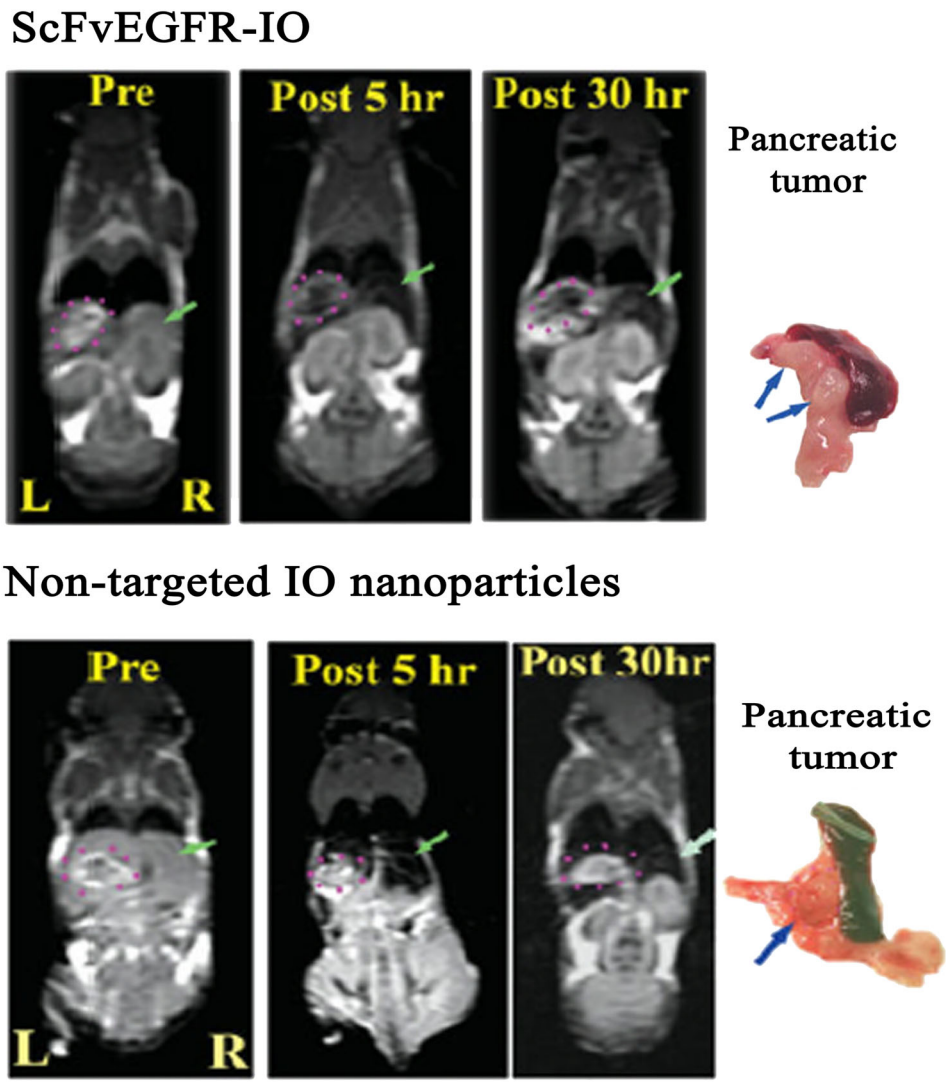

Figure 4. Target specificity of ScFv EGFR NPs by MRI using an orthotopic human pancreatic xenograft model: the areas of the pancreatic tumor are marked with a pink dashed circle. On the right is the picture of tumor and spleen tissues, showing sizes and locations of Q3 two intra-pancreatic tumor lesions (arrows) that correspond to the MRI tumor images. Reproduced with permission from Yang *et al*. (175).

xenografts, half an hour after injection, a considerable T_2 signal intensity could be noted. Therefore, the engineered probe was suggested to be a tool for evaluating the angiogenic state of lung cancer. Furthermore, some RGD mimetics have been synthesized and grafted onto NPs, and the resulting NPs have shown a good affinity for the $\alpha_v b_3$ integrins (190,191). Xie *et al*. (192) prepared SPIONs coated with 4-methylcatechol and further grafted with c(RGDyK) for targeting integrin $\alpha_v\beta_3$-rich human glioblastoma tumor cells (Fig. 5).

Aptamers are yet another class of targeting moieties made of single-stranded oligonucleotides, which are capable of recognizing their targets with high specificity and affinity. Indeed, due to their high specificity, aptamer-conjugated magnetic NPs have found several applications, for example in magnetic relaxation switches for detecting molecular interactions (193) and magnetic extraction of desired cells in a cell mixture (194,195). Yu *et al*. (196) synthesized SPIONs conjugated with a CG-rich duplex containing prostate-specific membrane antigen (PSMA) aptamer as theranostic agents against prostate cancer. Wang *et al*. have also described a study in which A10 RNA aptamers were conjugated to SPIONs via gel electrophoresis (197) and the nanosystem could release doxorubicin in a controlled fashion to PSMA-expressing PCa cells. Yigit *et al*. (198) prepared new adenosine DNA aptamer-functionalized SPIONs in a two-stage process via a reaction with SPDP and coupling with thiol-modified DNA. T_2-weighted MRI allowed the quantitative measurement of the adenosine concentration. A similar aptamer–SPION conjugate has also been fabricated for the detection of human α-thrombin in serum using MRI at concentrations below 25 nM (Fig. 6) (199). These representative studies demonstrate that aptamer–SPIONs can be used as potential theranostic agents.

4. CELLULAR IMAGING

4.1. Liver disease imaging

Liver diseases, encompassing hepatic fibrosis, microbial infections, and hepatocellular carcinoma (HCC), are a major public health burden worldwide (200). The pathogenesis of hepatic fibrosis results from chronic liver injury, which is caused by chronic alcohol consumption, a viral infection such as hepatitis C or B, or fungal, bacterial, or parasite infections. Fibrosis is a

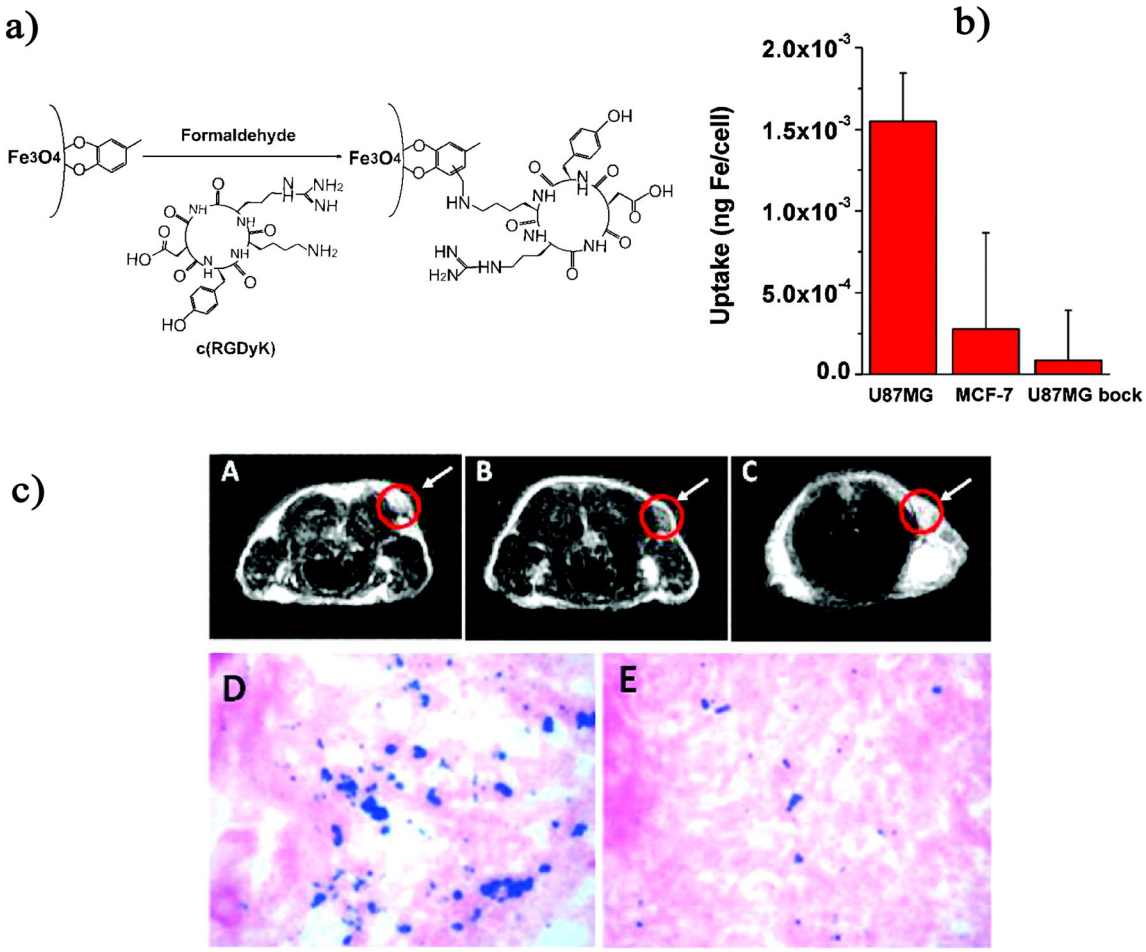

Figure 5. (a) Grafting c(RGDyK) peptide to superparamagnetic iron oxide NPs (SPIONs). (b) Cell uptake of c(RGDyK)-MC-SPIONs by U87MG, MCF-7, and U87MG+ c(RGDyK) block. (c) (A)–(C) MRI of the cross section of the U87MG tumors implanted in mice: (A) without SPIONs, (B) with the injection of 300 μg of c(RGDyK)-MC-SPIONs, and (C) with the injection of c(RGDyK)-MC-SPIONs and a blocking dose of c(RGDyK); (D), (E) Prussian blue staining of U87MG tumors in the presence of (D) c(RGDyK)-MC-SPIONs and (E) c(RGDyK)-MC-SPIONs plus a blocking dose of c(RGDyK). Reproduced with permission from Xie *et al*. (192). Copyright (2008) American Chemical Society.

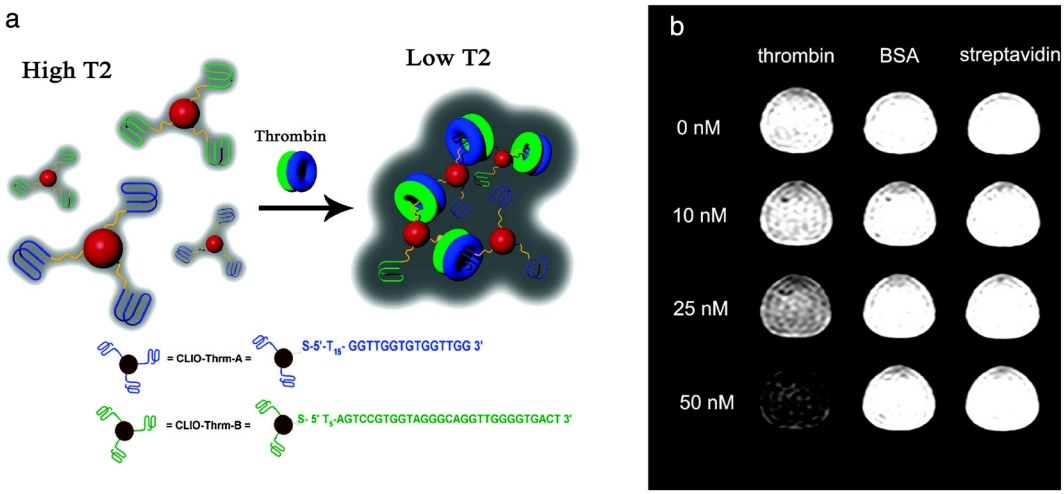

Figure 6. (a) The cross-linked iron oxide (CLIO) NPs (shown as red spheres) were modified with either Thrm-A, a DNA aptamer (shown as blue lines) that binds to the fibrinogen-recognition exosite of thrombin, or Thrm-B, a DNA aptamer (shown as green lines) that binds to the heparin-binding exosite of thrombin. Addition of thrombin consisting of both fibrinogen (as blue rings) and heparin (as green rings) exosites resulted in aggregation of CLIO NP assembly, reducing the T_2 relaxation time. The DNA sequences are shown at the bottom. The drawing is not to scale. (b) Contrast change in T_2-weighted MR image in 1:1 CLIO–Thrm-A and CLIO–Thrm-B mixture with 0, 10, 25, and 50 nM thrombin, bovine serum albumin, and streptavidin. Reproduced with permission from Yigit *et al*. (199). Copyright (2008) USA.

scarring process associated with the excessive accumulation of extracellular matrix proteins including collagen, proteoglycans, and other macromolecules. Finally, advanced liver fibrosis results in cirrhosis and liver failure that necessitates liver transplantation (201). On the other hand, chronic viral hepatitis most commonly turns into HCC, which is the third most common cause of death from cancer in the world.

Currently, the histological examination of a liver biopsy is the standard reference method for the diagnosis and staging of liver fibrosis. However, histology suffers from invasiveness and sampling variability and may introduce complications. These factors make histology unsuitable for both the diagnosis and longitudinal monitoring of liver fibrosis (202). A range of MRI-based techniques have been used for diagnostic and treatment-monitoring purposes in chronic liver diseases. Although conventional MRI is capable of visualizing morphological alterations in the liver, such as surface nodularity and the widening of fissures, it fails to clearly visualize the fibrosis itself (202). As an alternative, contrast-enhanced MRI provides cellular-level information about different types of liver tissue abnormality, such as fibrosis (200). SPIONs have been widely used as contrast agents in hepatic imaging.

Liver cellular imaging using SPIONs is mainly based on passive imaging, which relies on natural and rapid opsonization followed by the sequestration of SPIONs by Kupffer cells in the liver upon intravenous injection. Specialized macrophages of the RES, Kupffer cells, contribute to the normal physiology, homeostasis, and innate immune response of the liver. Because Kupffer cells contribute to the pathogenesis of several liver disorders, an imaging method that allows monitoring of the activity of Kupffer cells could provide valuable information in the diagnosis of liver status in healthy and diseased livers. For optimal opsonization and subsequent internalization by RES cells, SPIONs usually must have a large hydrodynamic size and preferably a hydrophobic or charged surface (203). Because healthy liver tissue has a higher SPION uptake than the fibrotic area (because of the reduced number of Kupffer cells), they accumulate more SPIONs, and thus the reduction of signal intensity on T_2-weighted images of normal parenchyma (204) is higher than in fibrotic areas. This fact forms the basis of detection by enhancing the contrast-to-noise ratio of the lesion and improving demarcation. Furthermore, this method can also be used for detection of most primary or metastatic liver tumors as hypointense signals, because they are also deficient in Kupffer cells and do not accumulate SPIONs (205). Many studies have thus coupled SPIONs with an MRI technique for imaging of different liver diseases. For example, a study reported the use of 193.8 nm alginate-coated SPIONs for visualization of hepatic lesions in a rodent model. After injection, 80% of the SPIONs accumulated in the liver, lowering the signal intensity in healthy liver and revealing a previously undetectable HCC in the rats (206). Interestingly, liver tumors can be detected even in the cirrhotic liver, where SPION uptake has been strongly impaired (207). Nevertheless, in some categories of hepatic lesions such as hepatocellular adenoma, focal nodular hyperplasia (FNH), dysplastic nodules (DN), and well-differentiated HCC, cells sustain phagocytic activity and they might demonstrate SPION accumulation and appear as isointense to normal liver tissue (208). For these patients, an MRI finding may not be precisely pathognomonic for the disease. Double contrast imaging using SPIONs and gadolinium-based contrast agents will enhance the clarity of liver lesions, especially for the detection of fibrosis. Because of the synergistic effect of signal reduction of background liver tissue by SPIONs and the enhancement of the signal of the water component within fibrotic tissue by gadolinium complexes, the visibility of liver fibrosis will be maximized (209). There are also several shortcomings associated with application of SPIONs for the cellular imaging of the liver. SPIONs are incapable of assessing lesion vascularity. Moreover, the decrease in signal intensity of the cirrhotic liver with SPIONs is limited compared with that in normal liver. In addition, lesion–liver contrast enhancement is weaker for HCCs arising in the cirrhotic liver than for hepatic metastases occurring in the normal liver. Finally, HCCs may contain a number of Kupffer cells, and some well-differentiated HCCs demonstrate a signal decrease after SPION administration.

Clinically available SPION formulations such as dextran-coated ferumoxides and Endorem® as well as carboxydextran-coated Ferucarbotran® were specifically approved for liver MRI. Because these formulations usually undergo nonspecific phagocytosis by Kupffer cells or other RES cells in the liver, spleen, and bone marrow after intravenous injection, imaging with these formulations demonstrates variable engulfment efficacy and is also limited to phagocytic cells (210).

Regarding the fact that the evaluation of the function of nonphagocytic hepatocytes plays an important role in clinical conditions such as liver transplantation or hepatitis, imaging the liver with hepatocyte-selective approaches is promising. The selective hepatocellular targeting can be controlled by modification of SPION surfaces with various targeting moieties such as antibodies, peptides, nucleic acids, or carbohydrates. Because hepatocytes have a high density per cell of asialoglycoprotein receptors (ASGP-Rs), which can bind to carbohydrates such as galactose, many SPIONs have been modified with carbohydrates for targeting purposes (211). For example, Lee *et al*. (212) have fabricated galactose-modified SPIONs, which were successfully used as a hepatocyte-targeted MRI and nuclear imaging contrast agent in a mouse model. In this study, the authors coupled lactobionic acid, a molecule with high affinity for ASGP-R, to dopamine-modified SPIONs labeled with ^{99m}Tc using NHS/EDC chemistry. Within a few minutes of tail vein injection, *in vivo* micro-SPECT/CT images and T_2-weighted MR images showed a high buildup of SPIONs in the liver, at a rate of 38.43 ± 6.45% injected dose per gram. Blocking the ASGP-R with free galactose significantly reduced the liver uptake of the SPIONs, indicating that the internalization of the NPs into hepatocytes is mediated by ASGP-R. The localization of lactobionic acid-SPIONs in liver tissue was also confirmed by TEM.

In addition to cancer imaging, SPIONs have been used as agents for the detection of cell death, as an early biomarker of the efficacy of anti-cancer treatments, and for the evaluation of tumor progression (213). Radermacher *et al*. (214) injected transplantable liver tumor (TLT) cells into the right gastrocnemius muscle of mice for the induction of tumors. As treatment, tumors were irradiated by an X-ray dose of 10 Gy to induce cell death. Then, pegylated SPIONs were coupled to apoptosis-recognizing moieties (PS-targeted E3 hexapeptide, peptide sequence: TLVSSL) and injected into mice at predetermined intervals. Peptide-grafted SPIONs exhibited selectivity for radiation-induced cell death compared with controls.

Despite the fact that SPIONs will naturally accumulate in liver upon intravenous injection, active targeting of SPIONs to liver macrophages has also been investigated. Vu-Quang *et al*. (215) reported on the use of β-glucan-coated SPIONs to diagnose liver

metastasis using MRI. β-glucan-modified NPs can target immune cells with the dectin-1 receptor. Using nonopsonic recognition, the specific interactions of these SPIONs with immune cells can be used for the precise detection of metastatic regions, which are devoid of immune cells.

Currently, the only curative treatment for a variety of acute and chronic liver diseases is liver transplantation. Thus, it is vital to evaluate hepatocyte integration within the liver parenchymal plates after intrasplenic and/or intraportal hepatocyte injection. SPIONs can be used to label cells for *in vivo* tracking applications. One of the easiest strategies is to co-incubate cells with SPIONs, where the NPs can be internalized through either spontaneous endocytosis or phagocytosis. Furthermore, functional biomolecules such as antibodies, transferrin, or HIV-tat peptide can be conjugated to SPIONs to further enhance their cellular uptake (216). However, this method has several complications. For example, it is difficult to distinguish single cells from clusters of cells and from contrast agent that has leaked from dead cells. Moreover, donor cell death or any leakage of SPIONs from transplanted hepatocytes can result in particle release followed by endocytosis by Kupffer cells or host hepatocytes in the liver, which makes it difficult to distinguish the fate of the transplanted cells. Luciani *et al*. (217) visualized the engraftment of intraportally injected mature mouse hepatocytes labeled with anionic SPIONs at 1.5 T. MRI images showed the presence of labeled cells in portal tracts and along liver sinusoids.

4.2. Gastrointestinal tract imaging

Chronic inflammatory bowel diseases, ulcerative colitis (UC), or Crohn's disease (CD) as well as gastric and colorectal cancer affect many people worldwide. MRI has great potential for the diagnosis and monitoring of the state of gastrointestinal (GI) diseases, involving the noninvasive evaluation of therapeutic outcomes (218). The application of conventional MRI in the study of GI diseases is limited by poor luminal contrast resolution. Because MRI contrast agents overcome this limitation, they are of paramount importance for the MRI of GI disorders (219). In MRI of GI disorders, the difference is that they are usually administered orally, unlike other cases, in which SPIONs are administered intravenously. These SPIONs help to distinguish bowel from intra-abdominal masses and normal organs, thus allowing for the accurate assessment of the luminal surface of the bowel wall (220). Two factors, namely 'thickness' and 'contrast enhancement' of the bowel, are normally used as markers for colitis in MRI studies. There are several preparations of SPIONs for use as oral MRI contrast agents, including AMI-121 (Lumirem by Guerbet and GastroMARK by Advanced Magnetics) and OMP (Abdoscan, Nycomed). These SPIONs are coated with nonbiodegradable and insoluble coatings such as siloxane and polystyrene. Furthermore, they are usually suspended in viscosity-increasing agents to prevent them from aggregating and digesting in the GI tract (221). In a recent study in a mouse model, D'Arienzo *et al*. (222) showed the high sensitivity of AMI-121 for the assessment of UC, providing comprehensive information on the colonic luminal surface and the bowel wall as well as the perivisceral structures. Even double contrast imaging agents, gadolinium complexes, could not be as informative as single oral contrast agents.

UC and CD normally exhibit uncontrolled inflammation in the small and/or large intestine, associated with the increased presence of neutrophils, natural killer cells, mast cells, and regulatory T cells. Elevated secretion of inflammatory species such as tumor necrosis factor alpha (TNF-α), interferon gamma (IFN-γ), interleukin (IL)-17, and matrix metalloproteinase can induce the degradation of the lamina propria or deeper tissue layers such as submucosa, muscularis, and serosa in the intestine (223). In UC and CD, bowels are infiltrated with inflammatory cells that can take up SPIONs, allowing their accumulation in the inflamed area. SPION-enhanced MRI can differentiate between nonspecific swelling and inflammatory regions in the bowel.

The risk of colon cancer is higher for patients with UC and CD. For these patients, the cumulative exposure to ionizing radiation during diagnosis, treatment, and subsequent monitoring can be substantial. Therefore, cell-specific MRI can provide a much safer alternative for such patients. For imaging of the colon using orally administered SPIONs, these particles should be efficiently internalized and subsequently transported by colon cells into deep layers of the tissue. However, the challenge is to allow efficient transport of SPIONs through the GI barrier, a first barrier through which orally delivered SPIONs must traverse. The GI barrier is a complex network of epithelial cells and tight junctions, which, along with secretions and other influences, controls the efficient transport of nutrients across the epithelium while strictly preventing the passage of unsafe molecules into the animal (224). So far, few studies have focused on the evaluation of SPION uptake and transport by human colon cells. Kenzaoui *et al*. (225) investigated the association of surface characteristics of SPIONs with their uptake and transport across human colon cells. More specifically, they developed a three-dimensional rounded spheroid model system of HT-29 or Caco-2 cells and evaluated the uptake of cationic amino-PVA-coated SPIONs and anionic oleic acid-coated SPIONs. As expected, the SPIONs demonstrated different uptake behavior. Although amino-PVA–SPIONs penetrated deep into Caco-2 and HT-29 spheroids, oleic acid-coated SPIONs were found in only the first cell layers of spheroids of Caco-2 cells. However, neither of the NPs could pass across the GI barriers. It must be considered that colon barrier models, such as the CacoReady or the CacoGoblet model, cannot truly test the ability of SPIONs to pass through diseased GI barriers. For example, because the barrier may represent a dysfunction in inflammatory bowel disease or colon cancer, SPION penetration and transportation may be facilitated and provide an opportunity for the imaging of colon disease.

4.3. Lymph node imaging

The spleen, thymus, adenoids, and tonsils constitute the human lymphatic system and are, in essence, a network of tissues and organs consisting of lymph nodes, lymph vessels, and lymph. (226). Diseases of the lymphatic system include Hodgkin's lymphoma, lymphangiosarcoma, lymphangioma, and lymphoma. Metastatic cancers of lymph nodes are considered as adverse prognostic factors in many types of cancer and are important in the staging of different types of cancer (227). Metastasis usually follows an orderly progression. Because the flow of lymph has an upright direction, the dissemination of cancer cells initially occurs in lymph nodes adjacent to the tumor site and in turn, other lymph nodes are engaged progressively. Therefore, the development of a noninvasive, tissue-specific, and highly sensitive imaging technique for assessing lymph node status will greatly help stage cancer, plan neoadjuvant therapy, and determine patient outcome (227,228). MRI is regarded as an attractive imaging modality for monitoring lymph node engagement,

especially in cancer. Despite the fact that measurement of nodal size by imaging is an accepted method for evaluation of nodal incursion by metastatic cells, the size criterion overlooks metastasis especially if micrometastasis is involved (229,230). An additional criterion, a morphological change of nodal glands to a more rounded shape after tumor infiltration, can also be used as a supporting factor for better diagnosis, but this also fails to reveal microscopic metastasis (96,231). Because SPIONs can target RES, they are among the favored contrast agents for lymph node imaging. Upon intravenous or subcutaneous injection, the distribution of SPIONs to the lymph nodes occurs by two distinct pathways. In the first pathway, SPIONs make their way to the lymph nodes via the high endothelial nodal venules followed by phagocytosis by macrophages. In the second pathway, SPIONs flow through transcapillary passage into the interstitium, where NPs are taken up by the draining lymphatic vessels and transported to the lymph nodes via afferent lymphatic channels (96,232,233). The physiochemical properties of SPIONs, e.g., size, surface charge, and coating, dictate their lymphatic trafficking to the lymph nodes (234). For example, SPIONs of less than 50 nm can migrate across the capillary wall and reach the lymph nodes, bone marrow, liver, and spleen, whereas SPIONs of 150 nm or more are usually observed only in the liver and spleen (96,226).

Ferumoxtran-10 is the first and most studied contrast agent for lymphatic imaging. In a healthy lymph node with normal function, macrophages would take up a large concentration of these NPs, leading to a shortening of T_2 and T_2* times, resulting in a marked decrease of signal intensity and darkening of the lymph nodes in MR images. Lymph nodes with infiltrated malignant tumors are devoid of macrophages, and they consequently lack uptake of ferumoxtran-10 and either remain isointense or display a heterogeneous signal intensity if only partial metastases or micrometastases are involved (231,235). Similarly, if metastases disturb the lymphatic flow, SPIONs cannot access the nodes, resulting in a hyperintense nodal image in MR. With a similar mechanism as described above, SPION-enhanced MRI can be used for differentiating normal tissues, hypercellular carcinoma, and neoplastic tissues in other lymphoid tissues, such as bone marrow and the spleen (236,237). SPION-enhanced MRI has been used for lymphatic mapping and sentinel node analysis and for the staging of different types of cancer (238). For example, Harisinghani *et al*. (239) reported that, in patients with T1-, T2- or T3-stage prostate cancer, SPION-enhanced MRI could determine all patients with nodal metastases and had a higher sensitivity than conventional MRI in a node by node analysis. Lymphotropic MR with SPIONs has been shown to improve nodal detection and sensitivity, specificity, and accuracy in other types of cancer such as bladder cancer (240), testicular cancer (241), penile cancer (242), esophageal cancer (243), and rectal cancer (244), as well as endometrial and cervical cancer (245).

Lymph nodes harbor a variety of immune cells such as T cells and B cells, which originate from bone marrow stem cells. T cells are not only involved in the pathogenesis of some autoimmune disorders, e.g. multiple sclerosis (MS), but they can also be recruited therapeutically in cancer immunotherapy. However, cell-based therapies for cancer are lagging and need a number of mechanistic amendments. In this context, MRI can be useful for its ability to visualize T cells and to possibly yield information on the molecular mechanisms of their recruitment. This can, in turn, open the possibility for early stage diagnosis of the disease and for optimization of cell therapies (246).

The earliest cellular MRI experiment relied on endocytotic labeling of rat T cells by dextran-coated SPIONs (AquaMag100 and BMS180549). Arbab *et al*. (247) also reported that dextran-coated SPIONs (ferumoxides) and protamine sulfate were effective for T cell labeling.

Dendritic cells (DCs) are also being considered for cancer immunotherapy. Upon activation, DCs migrate to the lymph nodes to interact with T cells and B cells, thus initiating the adaptive immune response. de Vries *et al*. (248) described an immunotherapeutic approach for patients with melanoma using autologous DCs. In this strategy, ferumoxide-labeled DCs were administered to patients under ultrasound guidance. Mature labeled DCs retained their phenotype, and no changes in their antigen-presentation and migration potential were noted. Furthermore, the cells were still positive for the DC marker S100. A 1:1 mixture of ^{111}In- and SPION-labeled autologous DCs was intranodally injected in eight patients with stage III melanoma. Subsequently, scintigraphy and MRI were both exploited to quantify and monitor the delivery of the DCs and their migration to proximal lymph nodes. Both the injection site and distant lymph nodes could be individually visualized on the MR image (3 T). Furthermore, the localization of SPIONs in the nodes was further confirmed using immunohistopathology, which showed the presence of iron-containing DCs in the paracortex and sinuses of the lymph node. Although the sensitivities of the two methods used in this study were almost equal, overall the authors concluded that MRI is superior to scintigraphic imaging because, in MRI, the delivery of the DC vaccine to the target location can be verified, cell tracking is more accurate, and DCs can be more precisely anatomically localized. Another study confirmed the possibility of using SPION-enhanced MRI for effectively tracking the *in vivo* migration of DCs (249).

4.4. Central nervous system disease imaging

Due to the complexity of the central nervous system (CNS), complications in the analysis of cerebrospinal fluid (CSF) and acquiring biopsies, as well as the relative inaccessibility of brain tissue in living models, imaging remains an important diagnostic tool for the identification of inflammatory loci, T staging of tumors, visualization of vascular structures, and anatomical examinations of the CNS (250,251). The small size of SPIONs allows them to carry therapeutics across physiological compartments in the CNS and may create the opportunity for simultaneous targeted therapy and imaging. Table 2 shows a brief description of CNS diseases and the pathological mechanisms involved.

Although the majority of the SPIONs are rapidly sequestered from the blood circulation by cells of the RES upon intravenous administration, circulating phagocytes also capture a small proportion of SPIONs in the blood. Regarding the fact that the common feature of CNS disorders such as MS, traumatic nerve injury, cerebral stoke, and brain tumors is the involvement of the immune system and inflammation (252), the engulfment of SPIONs with blood phagocytes can provide a tool for monitoring the involvement of macrophages in CNS diseases. MS is an inflammatory disease associated with demyelination and axonal loss in the CNS. Autoreactive T cells, T helper 1 cells, and macrophages usually have infiltrations in the MS lesions. Phagocytic microglia cells and blood-borne macrophages play key roles in the regulation of myelin attack and subsequent demyelination (253). The sensitivity of MRI for detecting single cells in the brain has been previously demonstrated (254). The current MRI contrast agent

Table 2. Some CNS diseases and their pathological mechanisms

Disease	Pathological mechanisms
Multiple sclerosis (MS)	Severe alteration of blood–brain barrier (BBB), loss of tight junctions, degradation of basal lamina, infiltration of T cells and macrophages, autoimmune response against myelin, chronic inflammation, oligodendrocyte cell death, and axonal damage (252).
Stroke	Cerebral ischemia through vascular obstruction initiated by inflammatory processes in the endothelial cells of the vessel wall. Drastic decrease in the supply of oxygen and glucose. Initiation of an ischemic cascade that involves necrotic cell death, apoptotic cell death, and an increased infiltration of monocytes and macrophages (363).
Alzheimer's disease (AD)	Accumulation of toxic aggregated amyloid fibrils, which induce apoptosis.Lesions of AD are associated with various inflammatory processes, which may have a secondary role to tissue damage.
Meningitis	Inflammation of meninges caused by viruses, bacteria, and microorganisms.
Epilepsy	Various causes; however, possible prolonged stimulation of pro-inflammatory signals, by seizures or a persistent pro-inflammatory situation in brain, may contribute to the establishment of a pathological substrate (364).
Brain tumors	Gliomas, meningiomas, pituitary adenomas, nerve sheath tumors.

for MS is a nonspecific Gd complex that can visualize blood–brain barrier (BBB) leakage (255). However, BBB leakage is only a consequence of the inflammatory process and not the inflammation itself. In contrast, transcytosis of SPIONs through the endothelial cell lining and uptake by local resident microglia or infiltration of activated blood monocytes that have phagocytosed SPIONs may allow for imaging of cellular infiltration and yields more information about inflammation and cellular involvement in MS (256,257). However, among the two mechanisms, SPION transcytosis is less probable, as recent studies have shown that under normal conditions nontargeted SPIONs have a very limited flux through the BBB (258,259).

In allergic encephalomyelitis (EAE) studies, MR enhancement from ferumoxtran-10 is different from that from Gd complexes. Although Gd MRI detects BBB leakage, cellular infiltration in MS lesions is related to macrophage infiltration reaching the brain parenchyma, and not to any alternate path. In all EAE studies, histological examinations have corroborated the MRI observation that SPIONs were mainly localized in macrophages in the CNS parenchyma (260–262). Accordingly, Bendszus *et al*. (263) showed that, after peripheral nerve injury in a rat model associated with macrophage infiltration, SPIONs were accumulated in degenerating sciatic nerves. In contrast, although SPION accumulation after optic nerve crush manifests microglial activation, macrophage infiltration is absent. Similar results have been observed in human studies. Using ferumoxtran-10 SPIONs, Dousset *et al*. (253) investigated whether monocyte/macrophage-labeled SPIONs infiltrate inflammatory MS brain lesions. Because SPIONs are too large to cross the BBB by passive diffusion, the transmigration of SPIONs was hypothesized to occur through SPION-loaded monocytes, which actively cross the BBB.

Another clinical application of SPIONs in cellular imaging is the evaluation of inflammation in cerebral ischemia. Ischemic stroke occurs because of a loss of blood supply to a part of the brain, initiating an intense local inflammatory response that involves microglial cell activation as well as infiltration by monocytes (264). Because these cells produce a wide spectrum of cytotoxic substances, they might aggravate the ischemic tissue damage. The main application of SPION-based MRI in stroke management is the visualization of the affected area, revealing the extent of the BBB breakdown and showing the movement and migration of immune cells inside the brain (265). Rausch *et al*. (262) studied SPION enhancement in a permanent middle cerebral artery occlusion (MCAO) model in rats. T_2-weighted MRI revealed the accumulation of activated macrophages in the periphery of the lesion area 24 h after the intravenous injection of Sinerem. Subsequent similar *in vivo* MR studies using a variety of SPIONs by Rausch *et al*. and Corot *et al*. (266,267) have shown the delayed onset of monocyte infiltration following ischemia in various rodent models. Histological examinations have also verified these findings, as it has been shown that blood-borne macrophages infiltrate the ischemic area with a minimum delay of 24 h, followed by the main infiltration between 3 and 6 days (268). Following successful *in vivo* animal studies, Saleh *et al*. (269) pioneered the clinical MRI study of ischemic stroke in 10 patients using Sinerem 5–7 days after the onset of stroke. The cerebral MRI signal was in agreement with the expected distribution of macrophages and confirmed their infiltration from the peripheral blood. Nevertheless, for several reasons, there is no consensus on whether iron-containing cells in ischemic areas originate from circulating monocytes. First, due to the small size and neutral charge of the SPIONs, their uptake in monocytes is limited. Furthermore, early MR signal changes arise from SPION transfer through an impaired BBB or passive diffusion of free SPIONs and not by macrophage infiltration (270). A comparative study after the administration of mouse monocytes exogenously labeled with SPIONs and free SPIONs revealed a significant difference between the spatiotemporal distribution of SPIONs in the ischemic area, demonstrating that SPIONs in the brain may not be entirely introduced by monocyte infiltration (271). According to the results of subsequent studies using different labeling techniques and a MCAO stroke model, it was suggested that systemically administered SPIONs may be sequestered by RES cells and migrate to inflammation sites in the brain (270,272).

SPION-enhanced MRI is also used to study brain malignancies, which can be roughly classified as primary brain tumors that originate inside the brain and brain metastases that are initiated from primary tumors outside the CNS. Gliomas are the most common form of primary brain tumors. The tumor microenvironment harbors a heterogeneous set of cells including endothelial cells, which support angiogenesis, reactive astrocytes, and circulating inflammatory microglia and macrophages, which regularly penetrate tumors (273,274). Therefore, the differential occurrence of inflammatory cells within and around the tumor versus normal brain tissue may be exploited to label cells with SPIONs for tumor detection, tumor boundary delineation, and

tumor volume quantification (275,276). Zimmer *et al*. (277) reported on the intravenous injection of SPIONs in rats implanted with C6 glioma cells. All tumors became significantly hyperintense relative to brain tissue on T_1-weighted images. Small tumors showed a rather homogeneous hyperintensity, whereas a pattern of concentric rings was observed in larger tumors, corresponding to the macrophage infiltration profile. In a study comparing ferumoxides with ferumoxtran-10 in 20 patients with intracranial tumors, ferumoxtran-10 outperformed ferumoxides in the imaging of intracranial tumors. Fleige *et al*. (278) reported a similar finding that SPION-labeled microglia can precisely show tumor morphology using *in vivo* MRI.

SPIONs can be alternatively used for noninvasive *in vivo* imaging of post-stroke recovery of the brain after cell-based therapies (279). This topic will be elaborated further in the stem cell labeling section.

4.5. Cardiovascular disease imaging

Cardiovascular conditions are the leading cause of death worldwide. Atherosclerosis and hypertension are the two most common underlying causes of cardiovascular disease. In atherosclerosis, the invasion of endothelium by oxidized plasma low-density lipoprotein (LDL) particles results in the initiation of an inflammatory response in the epithelial lining. This process is followed by the recruitment to the lesion-prone site of circulating monocytes, which then migrate to the sub-endothelial space and undergo further activation to form monocyte-derived macrophages (280). In a similar manner as discussed above, the presence of macrophages and phagocytosis of SPIONs could be used as markers of disease, here being specifically unstable atheromatous plaques. Cellular MRI is thus used to visualize the lesion-prone sites in the arteries (281,282). The passive accumulation of SPIONs in inflamed atheromatous plaques and a decreased focal signal intensity in the aortic wall have been clearly shown in animal studies (283–286). For example, Hyafil *et al*. (287) have used ferumoxtran-10 SPIONs and quantitative MRI to evaluate macrophage neointimal infiltration in hyper-cholesterolemic rabbit models with double-balloon injury of the infrarenal aorta.

In this context, macrophage accumulation in an inflamed artery can be used to estimate inflammation and stroke risk in patients. Preclinical studies have shown that ferumoxtran-10 can be used for imaging carotid or aorta atheromatous plaques by inducing signal loss in MR images (288,289). Furthermore, another clinical study confirmed that the macrophages residing in stenotic carotid plaques can capture ferumoxtran-10 (290). In spite of this, MRI may not be as successful in the detection of inflammation in smaller vessels, such as coronary arteries, because it is tricky to distinguish signal loss caused by SPIONs from the dark vessel lumen in small-diameter vessels (291).

Several SPION parameters such as size, nature, charge, coating, and the target cell type determine the extent of NP uptake. Although, for example, phagocytic cells internalize large particles more effectively than small ones, nonphagocytic T cells internalize intermediate-sized particles more efficiently (292–294). Overall, SPION uptake and MR enhancement depend on the type of contrast agent and animal model used. For example, Herborn *et al*. (295) showed that, though ferumoxtran-10 particles are larger than those of ferumoxytol, it had the highest luminal signal intensity on day 5, and that it was only 3 days for ferumoxytol.

In a recent study, Tsuchiya *et al*. have compared the uptake by four different types of SPION, i.e. naked SPIONs, mannan-coated SPIONs, USPIONs, and mannan-coated USPIONs, in the rabbit atherosclerotic wall. Histological and imaging analysis revealed that mannan-coated SPIONs and USPIONs have much faster uptake rates in the atherosclerotic rabbit wall than in the uncoated counterparts. Iron-positive regions were significantly larger with mannan-coated particles, whereas USPIONs had higher internalization in macrophages than SPIONs. Regarding the fact that immune cells, including macrophages and monocyte-derived DCs, express the mannose receptor, coating SPIONs with mannan increased their affinity for active atherosclerotic plaques, most likely by targeting the mannose receptors (296). The optimum time course for *in vivo* macrophage visualization using SPIONs in symptomatic human carotid disease has been reported to be between 24 and 36 h after SPION (Sinerem) infusion (290). In addition, SPIONs might be helpful in imaging aneurysms, especially those at an increased risk of growth or rupture (297). Because abdominal aortic aneurysms have an underlying inflammatory cause, SPION-enhanced MRI can be potentially effective in the visualization and assessment of the severity of the aneurysms.

Yet another application of SPIONs in the domain of cardiovascular disease is imaging inflammatory processes in myocardial infarction (MI). Not only is this important for the noninvasive *in vivo* assessment of cellular myocardial inflammation as well as the healing and regeneration process, but it also helps evaluate the potential efficacy of therapeutic interventions. Richards *et al*. reported the use of ferumoxides with rapid removal from the blood stream for *ex vivo* labeling of human monocytes. After labeling of monocytes, their homing to the infarcted area was visualized. In this study, the authors showed that, although injected cells retained their viability, they were able to migrate to inflammation sites, as confirmed by tuberculin skin testing. Subsequently, SPION-labeled cells could be clearly detected with T_2*-weighted MRI and R_2* maps (298). In addition to monitoring cell myocardial inflammation, SPIONs have been used for the noninvasive monitoring of inflammatory changes associated with cardiac graft rejection.

To further increase the accuracy of MRI, this imaging method can be further coupled with other imaging modalities. For example, magneto-fluorescent NPs have been used for simultaneous MRI and fluorescent molecular tomography (299).

To further enhance the capability of SPION-based formulations to target and witness molecular events *in vivo*, the surface of these NPs can be modified with targeting moieties. Cell adhesion molecules (CAMs) such as VCAM-1, ICAM-1, and selectin are attractive candidates for targeted nanosystems to activate the endothelium in vascular pathology (300). Tsourkas *et al*. (119) first described VCAM-1-targeted cross-linked SPIONs as diagnostic agents for vascular inflammation. In this study, Cy5.5-SPION conjugated to VCAM-1 monoclonal antibodies demonstrated the feasibility of the *in vivo* imaging of VCAM-1 expression in TNF-α-stimulated mouse ear vasculature. In another study, McAteer *et al*. (301) used iron oxide microparticles targeting VCAM-1 in mouse models of cerebral inflammation induced by TNF. MRI detected enhanced uptake of anti-VCAM-1 antibody-coated microparticles in the animals (301,302). As an alternative to antibody targeting, VCAM-1 targeting peptides, identified by phage display, can be used (122,299). For instance, SPIONs conjugated to a VCAM-1-specific cyclic peptide have been recently prepared for the *in vivo* detection of vascular inflammation in

early and advanced atherosclerotic plaques in ultra-high-field strength MRI (17.6 T) (303). In a recent study on mice, peptides with an affinity for VCAM-1 and apoptosis were used for the functionalization of USPIONs (304), which enabled the particles to report on distinct biological processes after co-localization in the plaque.

4.6. Imaging of infection

When bacterial infection occurs, phagocytes are activated and migrate to the infection site and activate the inflammatory cells by releasing cytokines. Targeting infection sites *in vivo* is a challenge; one reason for this is that most of the SPIONs with a size of approximately 150 nm are opsonized and subsequently phagocytosed by Kupffer cells and the mononuclear phagocytic system of the spleen. A smaller fraction of SPIONs with a longer blood circulation time eventually end up in the RES of liver and spleen. A few residual particles may randomly escape into the infarcted area due to the endothelial rupture and the increase in the vessel permeability and be subsequently engulfed by phagocytes (305). Gellissen *et al*. (306) used 26 nm PEG-coated Fe_3O_4 for infection monitoring up to a 60 min time delay after SPION administration. The steric hindrance provided by PEG coating inhibits opsonization and prolongs the blood circulation time of SPIONs. A model of infection was created by injecting *Staphylococcus aureus* into the right peritibial soft tissue of rats. The loss of signal intensity observed in inflamed tissue outside the RES was attributed to a net effect of perfusion, extravasation, and phagocytosis of SPIONs. The presence of interstitial iron deposits in proximity to the abscesses proves the transcapillary transport of SPIONs. In another study, Kaim *et al*. (307) reported on the visualization of infection in rats with ferumoxtran-based MRI, by creating an abscess via injection of *S. aureus* into unilateral deep calf muscle. Animals were imaged at different times to monitor acute, early chronic, and late chronic infection. A significant decrease in T_2-relative signal intensity was found at 24 h, reflecting intracellular iron accumulation within macrophages. Lee *et al*. (308) also used MRI to study induced infectious arthritis of the knee or soft tissue in rats. The authors employed 62 nm SPIONs to avoid entrapment in the RES of the liver and spleen. A signal loss in T_2-weighted images characteristic of abscesses in soft tissue was found 4–7 days following SPION injection.

Baraki *et al*. (309) labeled neutrophil granulocytes, the first phagocytizing cells that penetrate and access infected tissue *ex vivo*, with FeraTrack™ SPIONs and injected them in rats inoculated with a subcutaneous *S. aureus* suspension in the left parasternal chest area. Signal loss in MR images confirmed the migration of granulocytes to the infected tissue. The sensitivity of this technique, however, remains limited to the detection of acute infection, because chronic infection is associated more with the recruitment of macrophages and lymphocytes rather than granulocytes. In a recent study, Hoerr *et al*. (310) have devised a new *in vivo* imaging platform based on MRI for tracking infectious bacteria in mouse models, to increase the understanding of infection biology. SPIONs were used for labeling Gram-positive and Gram-negative bacteria, which were then injected subcutaneously or systemically to induce the infection model. MR images could be used for bacterial tracking and showed that labeled bacteria injected in the foot pad migrate to the popliteal lymph node, resulting in hypointensities in this area. In another study, Bierry *et al*. (311) employed macrophage imaging based on SPION-enhanced MRI to differentiate between infectious vertebral osteomyelitis and aseptic inflammation associated with degenerative intervertebral disk endplates in human patients. This strategy was based on the difference in macrophage distribution between vertebral infection and aseptic disk inflammation. Inflammation is usually associated with an acute, neutrophil-dominated response followed by recruitment of macrophages for the removal of cellular debris and the induction of the repair cascade. Thus, in inflammation, fibroblasts and lymphocytes form the major cellular infiltrations and macrophages account for only 10% of the cells. However, in the case of infection, macrophages are constantly recruited to the bone marrow and attracted to the infection sites due to the presence of infectious agent. The results of T_2 MRI in the infection group demonstrated a significant loss of abnormal endplates, but in the degenerative spine group no significant signal loss was noted in either T_2 or T_1 MR images.

4.7. Arthritis imaging

Arthritis generally refers to the inflammation of joints. The most common form, osteoarthritis, is a degenerative joint disease that occurs due to trauma, infection, overuse, or age. Because the degeneration of cartilage results in the recruitment of inflammatory cells to remove debris, osteoarthritis is associated with mild inflammation (312). Another form of arthritis is rheumatoid arthritis, which is a systemic autoimmune inflammatory disease with synovial involvement. Simon *et al*. (313) investigated the ability of SHU 555 C, ferumoxtran-10, and ferumoxytol to detect and characterize antigen-induced arthritis using MRI. Interestingly, despite differences in size, charge, and coating, all three SPION preparations provided a marked and prolonged positive enhancement in early post-contrast T_1-weighted MR images and a persistent negative enhancement in delayed T_2/T_2*-weighted MR images, reflecting the uptake in activated macrophages in arthritic knees.

4.8. Imaging of cell migration and cell trafficking

Due to their efficiency in MRI enhancement, general safety, and biodegradability through the iron metabolism pathways (314,315), magnetic NPs represent efficient cell labels for cellular imaging. For cell tracking studies, cells must be initially labeled with magnetic NPs. However, because the cellular internalization of most SPIONs is poor, transfection agents have been proposed to enhance the internalization efficiency (for more detailed information about labeling methods refer to Fig. 7). The complex of SPIONs such as ferumoxtran and ferumoxides with polycationic transfection agents has been extensively used to effectively label cells (316–323). For example, ferumoxides and protamine sulfate, both FDA-approved agents, can make a complex for the efficient and effective labeling of stem cells (318,319,324–326). The generated complex is then internalized into cells via macropinocytosis and can be visualized at clinical MRI fields. The final iron content of cells is dictated by several factors, including the nuclear/cytoplasm ratio and the number of incorporated NPs; the latter is related to the incubation time and the method of endocytosis (317,318). The difference in the iron content of labeled cells from that of the surrounding tissue helps track the cells *in vivo*. Although each unlabeled stem cell has only 0.1 pg of iron, a labeled suspension of cells such as monocytes can take up to 1–5 pg iron per cell, and adherent cells can usually

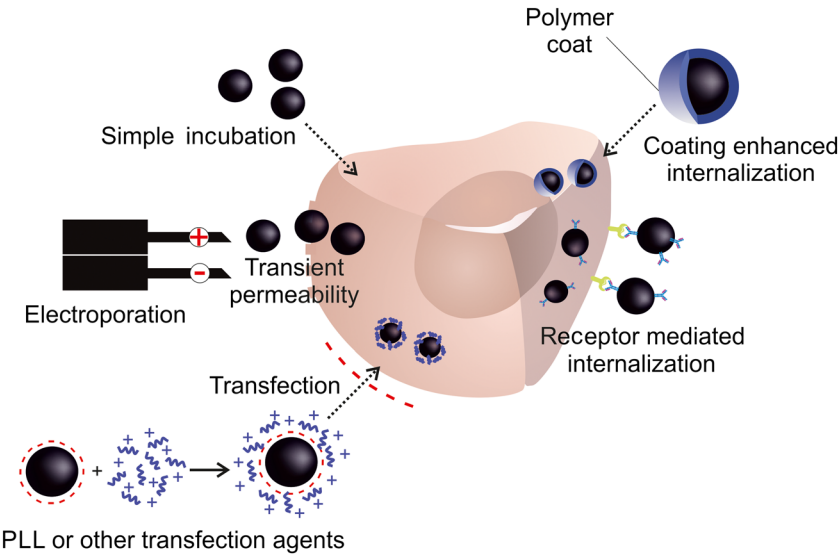

Figure 7. Different methods for stem cell labeling: simple incubation (poor efficiency, relatively long time), coating-enhanced internalizations, receptor-mediated internalizations (very specific and achieved by functionalization with targeting molecules such as antibodies and peptides), using transfection agents such as PLL (transfection), and electroporation (quick method based on induction of transient porosity in the membrane).

internalize from 5 up to more than 20 pg iron per cell (318,319,327–329). Labeled cells have been tracked by clinical MRI systems in different animal models (327–329). In most of the pilot studies, cells were usually labeled with FDA-approved SPIONs so that subsequent clinical trials could circumvent the problem of toxicity issues to the formulation constituents if possible. Owing to the susceptibility effect of SPIONs, MRI can readily detect labeled cells with a higher efficiency than cells labeled with gadolinium or T_1-based MRI contrast agents.

Several strategies have been employed to enhance cell labeling with MRI probes. In one of these techniques, the surface charge of the NPs is rendered positive by coating them with cationic materials. For this purpose, dextran and/or crosslinked dextran, dendrimers, starch, and citrate can be attached through electrostatic interactions to the SPION surface (60).

Ferumoxides, ferucarbotran, and ferumoxtran-10 are among the dextran-coated SPIONs that have been used for cell labeling (240,330–333). Moreover, cationic coating with carboxypropyl trimethyl ammonium (WSIO) and citrate (VSOP C184) can facilitate SPION incorporation into endosomes in macrophages (334). In another study, Bulte *et al.* (334) coated NPs with PAMAM dendrimer ($G = 4.5$) to facilitate their cellular uptake. Subsequent transplantation of the labeled NPs into the ventricles of neonatal dysmyelinated Long Evans shaker rats as well as their translocation into the brain parenchyma could be monitored using MRI over 42 days post implantation.

In another strategy, membrane-penetrable peptides can be used to modify the surface of NPs for optimal cell labeling. Conjugating SPIONs with TAT peptide has been shown to remarkably enhance the intracellular magnetic labeling of different target cells, including murine lymphocytes, human natural killer cells, and the HeLa cell line (336). For example, in one study (337), the sulfhydryl groups of SPIONs cross-linked with N-succinimidyl-3-(2-pyridyldithio)propionate were used for the conjugation of fluorescent TAT–FITC (fluorescein isothiocyanate) peptides. Subsequently, upon injection, the SPION–TAT-labeled lymphocytes could be located in the liver and spleen in mice.

Apart from peptides, NPs may also be functionalized with other specific antibodies and antibody fragments for improving internalization efficiency (338). For example, in a study by Bulte *et al.* (339), SPIONs conjugated with monoclonal antibody OX-26 against rat transferrin receptor were used to label rat progenitor oligodendrocytes. The labeled cells were subsequently transplanted into the spinal cords of myelin-deficient rats. The results of *ex vivo* MRI were closely correlated with the degree of myelination in the spinal cord 10–14 days post-transplantation.

4.9. Stem cell labeling

Self-renewal and differentiation into a variety of mature cell lines are the most important features of stem cells required for growth, development, and repair in multicellular organisms (340). Stem cells are normally classified as embryonic stem cells (ESCs), induced pluripotent stem cells (iPSCs), or postnatal adult stem cells (341). Acquired from the inner mass of blastocysts, ESCs can differentiate into almost any type of mature cell except for those in extra-embryonic tissue (340). iPSCs result from the reprogramming of differentiated human somatic cells to a pluripotent state (342).

Adult mesenchymal stem cells (MSCs) are derived from bone marrow and are of great promise and importance for the regeneration of damaged/diseased mesenchymal tissues (343). As mentioned above, SPIONs are the most widely used contrast agents for the detection of implanted cells *in vivo*. In this context, SPION-labeled stem cells have the potential to increase our knowledge and understanding of post-transplantation cell behavior and migration processes under a variety of conditions. Furthermore, the information obtained from cell tracking investigations can have great implications for the differentiation of stem cells/progenitor cells. That is, under certain conditions, transplanted SPION-labeled cells can be isolated via magnetic separation to investigate the differentiation of these cells upon exposure to a particular biological environment (344).

4.9.1. Stem cell labeling for orthopedic applications

4.9.1.1. Cartilage regeneration. Because cartilage has no vasculature or drainage, it suffers from poor self-regeneration capacity. Trauma, osteoarthritis, and rheumatoid arthritis normally

give rise to cartilage defects (345). Stem cell therapies have created the hope of restoring the functional properties of damaged cartilage via their regenerative capacity (346). Bone marrow-derived MSCs and chondrocytes are the two main cell types used for cartilage regeneration applications. SPION labeling can be used to study the *in vivo* fate of these cells after transplantation and to assess their degree of survival and integration into the target tissue. Jing *et al.* (345) labeled rabbit MSCs with SPIONs (Feridex IV) using protamine sulfate and injected these cells into defective cartilage in a rabbit model. All of the rabbits underwent gradient-recalled echo (GRE) T_2*-weighed MRI over a 12 week period post injection. Although MSC migration to the synovial fluid at the suprapatellar bursa, the popliteal space site, and the subchondral bone of the femur was noted 12 weeks after injection, no MSCs were present in the defect. Given these results, the authors suggested that, upon intra-articular injection, autologous MSCs do not actively engage in the repair of articular cartilage defects.

4.9.1.2. Intervertebral disk regeneration. In a degenerated disk, inflammatory and catabolic processes reduce the intrinsic regenerative and reparative capacity of cells. In these cases, engraftment of healthy stem cells into the degenerated intervertebral disk might be able to resolve the issue by restoring the function of disk to normal levels. Because an intervertebral disk has very limited access to systemic circulation and nutrients (347), it can hardly maintain the viability of transplanted cells, and thus tracking the fate of transplanted stem cells is very important. In one study, Jiang *et al.* (348) used MRI to study the *in vivo* trafficking of SPION-labeled adipose-derived stem cells as well as their efficacy in repairing degenerated intervertebral disks in rabbits. The results of this study indicated that stem cells are effective in regeneration of degenerated intervertebral disks.

4.9.1.3. Bone tissue engineering. The development of tissue engineering approaches holds great promise, especially for the repair of large bone defects. In bone tissue engineering, autologous cells are seeded in a three-dimensional scaffold, and subsequent implantation of this construct into the bone defect can give rise to new bone tissue that is highly similar to the surrounding bone in terms of structure and function (349). To this end, Lalande *et al.* (349) seeded SPIONs and rhodamine-labeled human adipose-derived stem cells within a polysaccharide-based three-dimensional scaffold. MRI was capable of detecting the labeled cells in the cellularized scaffolds implanted subcutaneously in nude mice for over 28 days. During this period, MRI could successfully confirm the retention of cells, their migration from the scaffold, and their colonization. The loss of signal intensity in the center of the scaffold after 7 days was attributed to cell death in the center of the scaffold and NP release in the periphery of the implant. Overall, it was shown that MRI is a valuable tool for monitoring the integration of a tissue-engineered construct into the surrounding tissue.

4.9.2. Stem cell labeling for cardiovascular diseases

Ischemic heart disease is the most common cause of death in industrialized countries (350). Human ESCs (hESCs) are regarded as novel promising therapeutic candidates for regenerative treatment of heart diseases. In this context, tracking transplanted cells *in vivo* can greatly improve our understanding of the mechanisms of heart repair and regeneration following treatment. Tallheden *et al.* (351) transplanted hESCs labeled with dextran-coated SPIONs into an explanted mouse heart *ex vivo* and injected them into the anterior left ventricle of rats *in vivo*. Although heart motion artifacts blur the results of MRI, the authors succeeded in visualizing the magnetically tagged cells *in vivo*.

In all studies that involve labeling stem cells with SPIONs, preliminary studies must be carried out to evaluate the effect of the labeling agent and procedures on the biological properties and the differentiation potential of the stem cells. For example, the impact of SPION labeling on the cardiac differentiation potential of ESCs has been evaluated by Au *et al.* (352) in an acute MI model in mice. *In vitro* studies showed that the viability and differentiation of ESCs was not affected by SPION labeling. No difference was observed between the calcium transients of SPION-labeled cells and those of their nonlabeled counterparts with respect to amplitude, maximal upstroke velocity, and maximal decay velocity. During *in vivo* experiments, the animals were intramyocardially injected with SPION-labeled nondifferentiated ESCs, and their progress was monitored using 7.0 T MRI over 10 days post injection. The injected ESCs were shown to significantly improve the left ventricular ejection fraction and, more importantly, at the injection sites in the ESCs group, areas of well-defined hypo-intensities were observed, but no such areas were detectable in control groups. Histological analysis of these hypo-intense regions also confirmed the *in vivo* cardiac differentiation of ESCs.

Upon injection to post-infarcted animal heart, bone marrow stem cells differentiate into three major cell types: cardiomyocytes, smooth muscle cells, and endothelial cells. Induction of neoangiogenesis by these cells results in the restoration of cardiac function. In one study, bone marrow-derived stem cells labeled with micrometer-sized iron oxide particles were grafted in rats *in vivo* and the cardiac function was monitored noninvasively using 11.7 T MRI (353). The stem cells were labeled with chloromethyl-benzamidodialkyl carbocyanine (CM-DiI) cell tracker dye and incubated overnight with microparticles (2 $\mu L/cm^2$) on the day before transplantation. Labeled cells were injected via either intramuscular or intravenous routes and tracked using MRI. It was observed that, upon direct injection of cells into the myocardium, the majority of cells remained in the vicinity of the injection site; in animals who received intravenous infusion, the cells were observed throughout the infarcted scar and were not visible in the myocardium. Although cells remained in the myocardium for up to 10 weeks post-injection, the stem cells did not improve the morphology or function of infarcted rat heart and did not increase neovascularization. Finally, the authors concluded that bone marrow-derived stem cells are not an ideal cell population for treatment of an infarcted heart.

In another study, Delo *et al.* (354) labeled human amniotic fluid stem cells (hAFSCs) with micrometer-sized iron oxide particles and investigated the fate of those cells following injection into mouse heart using 7.0 T MRI. They found that labeling does not affect the proliferation or differentiation of hAFSCs and that these cells were detectable *in vivo* up to 28 days post injection. Additionally, they showed that it would be possible to quantify the number of stem cells present at various time points according to the hypointensity volumes.

Wang *et al.* (355) also investigated the viability and function of adipose-derived stem cells (ADSCs) labeled with ferumoxides and evaluated whether the MR signal void resulting from SPIONs in live cells can be distinguished from that caused by dead cells *in vivo*. ADSCs were incubated with SPIONs for 2 days and then injected into an infarcted rat heart. Analysis of the cells 4 weeks post injection *in vivo* showed that the T_2* and T_2 relaxation times

of the labeled ADSCs correlated with the density and passage of cells. It was shown that signal voids in MR images represent the living cells.

Pluripotent stem cells have also been used to regenerate the infarcted heart *in situ*. It has been shown that a cardiopatch constituting bone morphogenetic protein-2 and SPION-labeled stem cells embedded into biodegradable fibrin matrices can provide a promising therapeutic strategy for cell implantation after cardiac infarction, as assessed for rat heart infarction (356). In this study, pluripotent stem cells were labeled with ferucarbotran via either lipofection or magnetofection and were tracked *in vivo* using 1.5 T MRI. Local and global heart functions of infarcted rat hearts together with the left ventricular dilation were remarkably improved within six weeks of cell transplantation.

4.9.3. Stem cell labeling for neurodegenerative diseases

4.9.3.1. Spinal cord regeneration. Currently, no therapeutic options exist for treatment of spinal cord injuries (SCIs), but recently stem cell therapies have engendered hope for improving the status of patients with SCI because stem cell transplantation in animal models has demonstrated an improved recovery after SCI. A wide source-independent variety of stem cells have been used for spinal cord transplantation. To translate these therapies to human clinical applications, several questions must be addressed, such as the best route for cell administration, the required number of cells to be transplanted, and the selection of the therapeutic window after injury. Stem cell tracking using SPION-based MRI can provide answers to these questions. The feasibility of tracking dual-labeled bone marrow MSCs, using adenovirus-carrying enhanced green fluorescent protein (AD5/F35-eGFP) and SPIONs, has been investigated in rats (9). The labeled stem cells were injected into rats with SCI through the subarachnoid space. MRI tracking results demonstrated that bone marrow MSCs migrated to the injured spinal cord over time and confirmed the utility of MRI for such applications. In another report (357), human $CD34^+$ umbilical cord blood stem cells labeled with SPIONs were injected into the spinal cord of a transgenic amyotrophic lateral sclerosis (ALS) mouse. *In vivo* imaging with 7.0 T MRI visualized the signals of implanted cells. Human umbilical cord MSCs (hUC-MSCs) also have been used for spinal cord regeneration. Hu *et al.* (358) labeled hUC-MSCs with SPIONs and subsequently injected them into rats with SCI. Rats receiving transplants were scanned using 7.0 T MRI up to 3 weeks post injection, and it was shown that transplanted cells can survive and migrate in the host tissue, promote function recovery, and produce a specific hypointense signal on MRI.

4.9.3.2. Brain. It has been suggested that neurological disorders (e.g. Parkinson's disease, stroke, etc.) might be ameliorated using stem cells. Animal studies have indicated that transplantation of stem cells in animals with strokes results in recovery; however, the mechanisms leading to these improvements are still not clear. An strategy using an induced inflammatory rat model was developed to assess the homing potential of neural crest stem cells and bone marrow-derived stem cells (359). The cells were first labeled with dextran-coated SPIONs and were further conjugated with FITC and TAT peptide. Afterwards, cells were either delivered either by direct implantation onto the corpus callosum or intravenous injection in animals with lesions. The labeled cells could be visualized as hypointense areas on T_2 MR images in the whole course of the study for up to 13 weeks. Interestingly in animals having a focal inflammatory lesion, the transplanted cells moved towards the lesion, and once at the site of lesion they stopped migration and remained visible on MRI for months. This migratory behavior was assumed to be due to the LPS-lesion model. The authors also mentioned that the signal void is mostly due to live cells, as the dead cells are cleared away from the local area.

Amyotrophic lateral sclerosis (ALS) is yet another disease for which treatment via regenerative medicine has been sought. This neurodegenerative condition results in muscular atrophy and paralysis by affecting upper and lower motor neurons (360).

Lu *et al.* (361) have tested the efficacy of intraarterial (IA) delivery of SPION-labeled MSCs in a canine stroke model. The transplanted cells could be visualized with 3.0 T MRI from even 1 h after transplantation up to four weeks afterwards. The majority of injected cells were found in the ipsilateral cerebral hemisphere of infarction, while only a few MSCs were detected in the contralateral side. The heterogeneity of brain hampers the exact determination of the number of cells.

Kallur *et al.* (362) tracked human neural stem cells obtained from the human fetal striatum in an *in vivo* model using MRI. For this purpose, cells were labeled with SPIONs (Endorem), injected unilaterally into the right striatum of neonatal rats and imaged with MRI for up to 16 weeks. A hypointense signal in the striatum was observed, which corresponded to the SPION-labeled cells. It was shown that the relative graft to brain volume ratio decreased by around 50% in 4 months. Moreover, a decrease in T_2 values was observed over time. According to post-mortem histological analysis and the fact that almost none of the grafted cells were proliferating after engraftment, the noted decline in T_2 values is not due to a dilution effect and might be due to cell migration from the graft core. However, since no obvious hypointensities were observed in the other regions of the brain, it was concluded that the T_2 decrease over time occurs as a result of changes based on development during brain growth.

5. CONCLUSION AND PERSPECTIVES

Recently, a great deal of effort has been focused on the application of NPs in molecular imaging and therapy. In this line, antibody- and peptide-conjugated NPs are being developed for the targeting of different disease states. Highly specific molecular and cellular MRI agents represent a noninvasive, nonionizing, and powerful tool to visualize physiological and pathological conditions. They have tremendous potential for improving our understanding of molecular processes involved in a variety of important clinical diseases. Finally, the novel applications of SPIONs, for example in stem cell tracking, have the potential to give us information about cell fate and migratory behavior after transplantation, and, as such, pave the way for clinical materialization of regenerative therapies.

Acknowledgements

SL thanks the Center for Microscopy and Molecular Imaging (CMMI, supported by the European Regional Development Fund and the Walloon Region). This work was supported by the Walloon Region (Program First spin-off), FNRS (Fond National de la Recherche Scientifique), UIAP VII and ARC Programs of the French Community of Belgium.

REFERENCES

1. Weissleder R, Ross BD, Rehemtulla A, Gambhir SS. Molecular Imaging: Principles and Practice. People's Medical Publishing House: Shelton, CT, USA, 2010.
2. Nolting DD, Gore JC, Pham W. Near-infrared dyes: probe development and applications in optical molecular imaging. Curr Org Synth 2011; 8(4): 521–534.
3. Modo MMJ, Bulte JWM. Molecular and Cellular MR Imaging. CRC Press: Boca Raton, FL, 2007.
4. Mahmoudi M, Serpooshan V, Laurent S. Engineered nanoparticles for biomolecular imaging. Nanoscale 2011; 3(8): 3007–3026.
5. Massoud TF, Gambhir SS. Molecular imaging in living subjects: seeing fundamental biological processes in a new light. Genes Dev 2003; 17(5): 545–580.
6. Debbage P, Jaschke W. Molecular imaging with nanoparticles: giant roles for dwarf actors. Histochem Cell Biol 2008; 130(5): 845–875.
7. Kiessling F, Liu Z, Gätjens J. Advanced nanomaterials in multimodal imaging: design, functionalization, and biomedical applications. J Nanomater 2010; 2010: 894303.
8. Rinck P. Magnetic Resonance in Medicine (4th ed). Wiley-Blackwell: Minusio, Switzerland, 2001.
9. Mahmoudi M, Stroeve P, Milani AS, Arbab SA. Superparamagnetic Iron Oxide Nanoparticles: Synthesis, Surface Engineering, Cytotoxicity and Biomedical Applications. Nova Science Publisher: New York, 2010, ISBN: 978-1-61668-964-3.
10. Vande Velde G, Baekelandt V, Dresselaers T, Himmelreich U. Magnetic resonance imaging and spectroscopy methods for molecular imaging. Q J Nucl Med Mol Imaging 2009; 53(6): 565–585.
11. Laurent S, Forge D, Port M, Roch A, Robic C, Vander Elst L, Muller RN. Magnetic iron oxide nanoparticles: synthesis, stabilization, vectorization, physicochemical characterizations and biological applications. Chem Rev 2008; 108(6): 2064–2110.
12. Mahmoudi M, Sant S, Wang B, Laurent S, Sen T. Superparamagnetic iron oxide nanoparticles (SPIONs): development, surface modification and applications in chemotherapy. Adv Drug Deliv Rev 2011; 63(1/2): 24–46.
13. Sharifi S, Behzadi S, Laurent S, Forrest ML, Stroeve P, Mahmoudi M. Toxicity of nanomaterials. Chem Soc Rev 2012; 41: 2323–2343.
14. Mahmoudi M, Hosseinkhani H, Hosseinkhani M, Boutry S, Simchi A, Journeay WS, Subramani K, Laurent S. Magnetic resonance imaging tracking of stem cells in vivo using iron oxide nanoparticles as a tool for the advancement of clinical regenerative medicine. Chem Rev 2011; 111(2): 253–280.
15. Mahmoudi M, Hofmann H, Rothen-Rutishauser B, Petri-Fink A. Assessing the in vitro and in vivo toxicity of superparamagnetic iron oxide nanoparticles. Chem Rev 2011; 112(4): 2323–2338.
16. Mahmoudi M, Laurent S, Shokrgozar MA, Hosseinkhani M. Toxicity evaluations of superparamagnetic iron oxide nanoparticles: cell 'vision' versus physicochemical properties of nanoparticles. ACS Nano 2011; 5(9): 7263–7276.
17. Mahmoudi M, Simchi A, Imani M. Cytotoxicity of uncoated and polyvinyl alcohol coated superparamagnetic iron oxide nanoparticles. J Phys Chem C 2009; 113(22): 9573–9580.
18. Amiri H, Mahmoudi M, Lascialfari A. Superparamagnetic colloidal nanocrystal clusters coated with polyethylene glycol fumarate: a possible novel theranostic agent. Nanoscale 2011; 3: 1022–1030.
19. Rauch J, Kolch W, Mahmoudi M. Cell type-specific activation of AKT and ERK signaling pathways by small negatively-charged magnetic nanoparticles. Sci Rep 2012; 2: 868.
20. Laurent S, Duts S, Hafeli U, Mahmoudi M. Magnetic fluid hyperthermia: focus on superparamagnetic iron oxide nanoparticles. Adv Colloid Interface Sci 2011; 166: 8–23.
21. Laurent S, Mahmoudi M. Superparamagnetic iron oxide nanoparticles: promises for diagnosis and treatment of cancer. Int J Mol Epidemiol Genet 2011; 2(4): 367.
22. Mahmoudi M, Sahraian MA, Shokrgozar MA, Laurent S. Superparamagnetic iron oxide nanoparticles: promises for diagnosis and treatment of multiple sclerosis. ACS Chem Neurosci 2011; 2(3): 118–140.
23. Hajipour MJ, Fromm KM, AkbarAshkarran A, Jimenez de Aberasturi D, Larramendi IRd, Rojo T, Serpooshan V, Parak WJ, Mahmoudi M. Antibacterial properties of nanoparticles. Trends Biotechnol 2012; 30(10): 499–511.
24. Laurent S, Saei AA, Behzadi S, Panahifar A, Mahmoudi M. Superparamagnetic iron oxide nanoparticles for delivery of therapeutic agents: opportunities and challenges. Expert Opin Drug Deliv 2014; 11(9): 1449–1470.
25. Corot C, Robert P, Idée JM, Port M. Recent advances in iron oxide nanocrystal technology for medical imaging. Adv Drug Deliv Rev 2006; 58(14): 1471–1504.
26. Laurent S, Bridot J-L, Elst LV, Muller RN. Magnetic iron oxide nanoparticles for biomedical applications. Future Med Chem 2010; 2(3): 427–449.
27. Mahmoudi M, Simchi A, Milani A, Stroeve P. Cell toxicity of superparamagnetic iron oxide nanoparticles. J Colloid Interface Sci 2009; 336(2): 510–518.
28. Lee N, Hyeon T. Designed synthesis of uniformly sized iron oxide nanoparticles for efficient magnetic resonance imaging contrast agents. Chem Soc Rev 2012; 41(7): 2575–2589.
29. Mornet S, Vasseur S, Grasset F, Duguet E. Magnetic nanoparticle design for medical diagnosis and therapy. J Mater Chem 2004; 14(14): 2161–2175.
30. Berry CC, Wells S, Charles S, Curtis ASG. Dextran and albumin derivatised iron oxide nanoparticles: influence on fibroblasts in vitro. Biomaterials 2003; 24(25): 4551–4557.
31. Lee K, Kim S-G, Kim W-S, Kim S. Properties of iron oxide particles prepared in the presence of dextran. Korean J Chem Eng 2002; 19(3): 480–485.
32. Laurent S, Nicotra C, Gossuin Y, Roch A, Ouakssim A, Vander Elst L, Cornant M, Soleil P, Muller RN. Influence of the length of the coating molecules on the nuclear magnetic relaxivity of superparamagnetic colloids. Phys Status Solididi C 2004; 1(12): 3644–3650.
33. Gamarra LF, Brito GES, Pontuschka WM, Amaro E, Parma AHC, Goya GF. Biocompatible superparamagnetic iron oxide nanoparticles used for contrast agents: a structural and magnetic study. J Magn Magn Mater 2005; 289: 439–441.
34. Paul KG, Frigo TB, Groman JY, Groman EV. Synthesis of ultrasmall superparamagnetic iron oxides using reduced polysaccharides. Bioconjugate Chem 2004; 15(2): 394–401.
35. Carmen Bautista M, Bomati-Miguel O, Del Puerto MM, Serna CJ, Veintemillas-Verdaguer S. Surface characterisation of dextran-coated iron oxide nanoparticles prepared by laser pyrolysis and coprecipitation. J Magn Magn Mater 2005; 293(1): 20–27.
36. Nishio Y, Yamada A, Ezaki K, Miyashita Y, Furukawa H, Horie K. Preparation and magnetometric characterization of iron oxide-containing alginate/poly(vinyl alcohol) networks. Polymer 2004; 45(21): 7129–7136.
37. Finotelli PV, Morales MA, Rocha-Leão MH, Baggio-Saitovitch EM, Rossi AM. Magnetic studies of iron(III) nanoparticles in alginate polymer for drug delivery applications. Mater Sci Eng C 2004; 24(5): 625–629.
38. Ma H-L, Qi X-R, Maitani Y, Nagai T. Preparation and characterization of superparamagnetic iron oxide nanoparticles stabilized by alginate. Int J Pharm 2007; 333(1/2): 177–186.
39. Morales MA, Finotelli PV, Coaquira JAH, Rocha-Leão MHM, Diaz-Aguila C, Baggio-Saitovitch EM, Rossi AM. In situ synthesis and magnetic studies of iron oxide nanoparticles in calcium-alginate matrix for biomedical applications. Mater Sci Eng C 2008; 28(2): 253–257.
40. Roohi F, Lohrke J, Ide A, Schütz G, Dassler K. Studying the effect of particle size and coating type on the blood kinetics of superparamagnetic iron oxide nanoparticles. Int J Nanomed 2012; 7: 4447–4458.
41. Burtea C, Laurent S, Mahieu I, Larbanoix L, Roch A, Port M, Rousseaux O, Ballet S, Murariu O, Toubeau G, Corot C, Vander Elst L, Muller RN. In vitro biomedical applications of functionalized iron oxide nanoparticles, including those not related to magnetic properties. Contrast Media Mol Imaging 2011; 6(4): 236–250.
42. Kim DK, Zhang Y, Kehr J, Klason T, Bjelke B, Muhammed M. Characterization and MRI study of surfactant-coated superparamagnetic nanoparticles administered into the rat brain. J Magn Magn Mater 2001; 225(1/2): 256–261.
43. Shultz MD, Calvin S, Fatouros PP, Morrison SA, Carpenter EE. Enhanced ferrite nanoparticles as MRI contrast agents. J Magn Magn Mater 2007; 311(1): 464–468.
44. Gupta AK, Curtis ASG. Surface modified superparamagnetic nanoparticles for drug delivery: interaction studies with human fibroblasts in culture. J Mater Sci Mater Med 2004; 15(4): 493–496.

45. Kohler N, Fryxell GE, Zhang M. A bifunctional poly(ethylene glycol) silane immobilized on metallic oxide-based nanoparticles for conjugation with cell targeting agents. J Am Chem Soc 2004; 126(23): 7206–7211.
46. Kellar KE, Fujii DK, Gunther WHH, Briley-Sabo K, Bjornerod A, Spiller M, Koenig SH. Important considerations in the design of iron oxide nanoparticles as contrast agents for T1-weighted MRI and MRA. Acad Radiol 2002; 9(Suppl. 1): S34–S37.
47. Acar HYC, Garaas RS, Syud F, Bonitatebus P, Kulkarni AM. Superparamagnetic nanoparticles stabilized by polymerized PEGylated coatings. J Magn Magn Mater 2005; 293(1): 1–7.
48. Ngaboni Okassa L, Marchais H, Douziech-Eyrolles L, Cohen-Jonathan S, Soucé M, Dubois P, Chourpa I. Development and characterization of sub-micron poly(d,l-lactide-co-glycolide) particles loaded with magnetite/maghemite nanoparticles. Int J Pharm 2005; 302(1/2): 187–196.
49. Sander EA, Alb AM, Nauman EA, Reed WF, Dee KC. Solvent effects on the microstructure and properties of 75/25 poly(D,L-lactide-co-glycolide) tissue scaffolds. J Biomed Mater Res A 2004; 70A(3): 506–513.
50. Kopke RD, Wassel RA, Mondalek F, Grady B, Chen K, Liu J, Gibson D, Dormer KJ. Magnetic nanoparticles: inner ear targeted molecule delivery and middle ear implant. Audiol Neurotol 2005; 11(2): 123–133.
51. Mornet S, Portier J, Duguet E. A method for synthesis and functionalization of ultrasmall superparamagnetic covalent carriers based on maghemite and dextran. J Magn Magn Mater 2005; 293(1): 127–134.
52. Duguet EMS, Portier J. French Patent FR2855315. Chem Abstr 2004; 141: 405023.
53. Wagner S, Schnorr J, Pilgrimm H, Hamm B, Taupitz M. Monomer-coated very small superparamagnetic iron oxide particles as contrast medium for magnetic resonance imaging: preclinical in vivo characterization. Invest Radiol 2002; 37(4): 167–177.
54. Taupitz M, Wagner S, Schnorr J, Kravec I, Pilgrimm H, Bergmann-Fritsch H, Hamm B. Phase I clinical evaluation of citrate-coated monocrystalline very small superparamagnetic iron oxide particles as a new contrast medium for magnetic resonance imaging. Invest Radiol 2004; 39(7): 394–405.
55. Fauconnier N, Pons JN, Roger J, Bee A. Thiolation of maghemite nanoparticles by dimercaptosuccinic acid. J Colloid Interface Sci 1997; 194(2): 427–433.
56. Fauconnier N, Bee A, Roger J, Pons JN. Adsorption of gluconic and citric acids on maghemite particles in aqueous medium. Prog Colloid Polym Sci 1996; 100: 212–216.
57. Fauconnier N, Bée A, Roger J, Pons JN. Synthesis of aqueous magnetic liquids by surface complexation of maghemite nanoparticles. J Mol Liquids 1999; 83(1–3): 233–242.
58. Jung CW. Surface properties of superparamagnetic iron oxide MR contrast agents: ferumoxides, ferumoxtran, ferumoxsil. Magn Reson Imaging 1995; 13(5): 675–691.
59. Cheng FY, Su CH, Yang YS, Yeh CS, Tsai CY, Wu CL, Wu MT, Shieh DB. Characterization of aqueous dispersions of Fe_3O_4 nanoparticles and their biomedical applications. Biomaterials 2005; 26(7): 729–738.
60. Jung CW, Jacobs P. Physical and chemical properties of superparamagnetic iron oxide MR contrast agents: ferumoxides, ferumoxtran, ferumoxsil. Magn Reson Imaging 1995; 13(5): 661–674.
61. Laurent S, Vander Elst L, Muller RN. Superparamagnetic iron oxide nanoparticles for MRI. In The Chemistry of Contrast Agents in Medical Magnetic Resonance Imaging (2nd edn). Wiley: Chichester, UK, 2013; 427–447.
62. Walczyk D, Bombelli FB, Monopoli MP, Lynch I, Dawson KA. What the cell 'sees' in bionanoscience. J Am Chem Soc 2010; 132(16): 5761–5768.
63. Lesniak A, Fenaroli F, Monopoli MP, Åberg C, Dawson KA, Salvati A. Effects of the presence or absence of a protein corona on silica nanoparticle uptake and impact on cells. ACS Nano 2012; 6(7): 5845–5857.
64. Monopoli MP, Walczyk D, Campbell A, Elia G, Lynch I, Baldelli Bombelli F, Dawson KA. Physical–chemical aspects of protein corona: relevance to in vitro and in vivo biological impacts of nanoparticles. J Am Chem Soc 2011; 133(8): 2525–2534.
65. Jedlovszky-Hajdú A, Bombelli FB, Monopoli MP, Tombácz E, Dawson KA. Surface coatings shape the protein corona of SPIONs with relevance to their application in vivo. Langmuir 2012; 28(42): 14983–14991.
66. Laurent S, Dutz S, Häfeli UO, Mahmoudi M. Magnetic fluid hyperthermia: focus on superparamagnetic iron oxide nanoparticles. Adv Colloid Interface Sci 2011; 166(1): 8–23.
67. Larbanoix L, Burtea C, Laurent S, Van Leuven F, Toubeau G, Elst LV, Muller RN. Potential amyloid plaque-specific peptides for the diagnosis of Alzheimer's disease. Neurobiol Aging 2010; 31(10): 1679–1689.
68. Abdolahi M, Shahbazi-Gahrouei D, Laurent S, Sermeus C, Firozian F, Allen BJ, Boutry S, Muller RN. Synthesis and *in vitro* evaluation of MR molecular imaging probes using J591 mAb-conjugated SPIONs for specific detection of prostate cancer. Contrast Media Mol Imaging 2013; 8(2): 175–184.
69. Mirshafiee V, Mahmoudi M, Lou K, Cheng J, Kraft ML. Protein corona significantly reduces active targeting yield. Chem Commun 2013; 49(25): 2557–2559.
70. Salvati A, Pitek AS, Monopoli MP, Prapainop K, Bombelli FB, Hristov DR, Kelly PM, Aberg C, Mahon E, Dawson KA. Transferrin-functionalized nanoparticles lose their targeting capabilities when a biomolecule corona adsorbs on the surface. Nat Nanotechnol 2013; 8(2): 137–143.
71. Amiri H, Bordonali L, Lascialfari A, Wan S, Monopoli MP, Lynch I, Laurent S, Mahmoudi M. Protein corona affects the relaxivity and MRI contrast efficiency of magnetic nanoparticles. Nanoscale 2013; 5(18): 8656–8665.
72. Wang J, Sui M, Fan W. Nanoparticles for tumor targeted therapies and their pharmacokinetics. Curr Drug Metab 2010; 11(2): 129–141.
73. Mahon E, Salvati A, Bombelli FB, Lynch I, Dawson KA. Designing the nanoparticle-biomolecule interface for "targeting and therapeutic delivery". J. Controlled Release 2012; 161: 164–174.
74. Vogl TJ, Hammerstingl R, Schwarz W, Mack MG, Müller PK, Pegios W, Keck H, Eibl-Eibesfeldt A, Hoelzl J, Woessmer B, Bergman C, Felix R. Superparamagnetic iron oxide-enhanced versus gadolinium-enhanced MR imaging for differential diagnosis of focal liver lesions. Radiology 1996; 198(3): 881–887.
75. Namkung S, Zech CJ, Helmberger T, Reiser MF, Schoenberg SO. Superparamagnetic iron oxide (SPIO)-enhanced liver MRI with ferucarbotran: efficacy for characterization of focal liver lesions. J Magn Reson Imaging 2007; 25(4): 755–765.
76. Wang YXJ, Hussain SM, Krestin GP. Superparamagnetic iron oxide contrast agents: physicochemical characteristics and applications in MR imaging. Eur Radiol 2001; 11(11): 2319–2331.
77. Gupta AK, Naregalkar RR, Vaidya VD, Gupta M. Recent advances on surface engineering of magnetic iron oxide nanoparticles and their biomedical applications. Nanomedicine 2007; 2(1): 23–39.
78. Semelka RC, Helmberger TKG. State of the art: contrast agents for MR imaging of the liver. Radiology 2001; 218(1): 27–38.
79. Weissleder R, Lee AS, Khaw BA, Shen T, Brady TJ. Antimyosin-labeled monocrystalline iron oxide allows detection of myocardial infarct: MR antibody imaging. Radiology 1992; 182(2): 381–385.
80. Suwa T, Ozawa S, Ueda M, Ando N, Kitajima M. Magnetic resonance imaging of esophageal squamous cell carcinoma using magnetite particles coated with anti-epidermal growth factor receptor antibody. Int J Cancer 1998; 75(4): 626–634.
81. Wadghiri YZ, Sigurdsson EM, Sadowski M, Elliott JI, Li Y, Scholtzova H, Tang CY, Aguinaldo G, Pappolla M, Duff K, Wisniewski T, Turnbull DH. Detection of Alzheimer's amyloid in transgenic mice using magnetic resonance microimaging. Magn Reson Med 2003; 50(2): 293–302.
82. Reimer P, Weissleder R, Shen T, Knoefel WT, Brady TJ. Pancreatic receptors: initial feasibility studies with a targeted contrast agent for MR imaging. Radiology 1994; 193(2): 527–531.
83. Jung HI, Kettunen MI, Davletov B, Brindle KM. Detection of apoptosis using the C2A domain of synaptotagmin I. Bioconjugate Chem 2004; 15(5): 983–987.
84. Artemov D, Mori N, Okollie B, Bhujwalla ZM. MR molecular imaging of the Her-2/neu receptor in breast cancer cells using targeted iron oxide nanoparticles. Magn Reson Med 2003; 49(3): 403–408.
85. Bulte JWM, Hoekstra Y, Kamman RL, Magin RL, Webb AG, Briggs RW, Go KG, Hulstaert CE, Miltenyi S, The TH, De Leij L. Specific MR imaging of human lymphocytes by monoclonal antibody-guided dextran-magnetite particles. Magn Reson Med 1992; 25(1): 148–157.
86. Go KG, Bulte JWM, De Ley L, The TH, Kamman RL, Hulstaert CE, Blaauw EH, Ma LD. Our approach towards developing a specific tumour-targeted MRI contrast agent for the brain. Eur J Radiol 1993; 16(3): 171–175.

87. Sun EY, Josephson L, Kelly KA, Weissleder R. Development of nanoparticle libraries for biosensing. Bioconjugate Chem 2006; 17(1): 109–113.
88. Renshaw PF, Owen CS, Evans AE, Leigh JS Jr. Immunospecific NMR contrast agents. Magn Reson Imaging 1986; 4(4): 351–357.
89. Suzuki M, Shinkai M, Kamihira M, Kobayashi T. Preparation and characteristics of magnetite-labelled antibody with the use of poly(ethylene glycol) derivatives. Biotechnol Appl Biochem 1995; 21(3): 335–345.
90. Zhou J, Leuschner C, Kumar C, Hormes JF, Soboyejo WO. Sub-cellular accumulation of magnetic nanoparticles in breast tumors and metastases. Biomaterials 2006; 27(9): 2001–2008.
91. Leuschner C, Kumar C, Urbina MO, Zhou J, Soboyejo W, Hansel W, Hormes F. The use of ligand conjugated superparamagnetic iron oxide nanoparticles (SPION) for early detection of metastases. Technical Proceedings of the 2005 NSTI Nanotechnology Conference and Trade Show, Vol. 1. Boca Raton, FL: CRC Press, 2007; 5–6.
92. Zhang C, Jugold M, Woenne EC, Lammers T, Morgenstern B, Mueller MM, Zentgraf H, Bock M, Eisenhut M, Semmler W, Kiessling F. Specific targeting of tumor angiogenesis by RGD-conjugated ultrasmall superparamagnetic iron oxide particles using a clinical 1.5-T magnetic resonance scanner. Cancer Res 2007; 67(4): 1555–1562.
93. Peng ZG, Hidajat K, Uddin MS. Adsorption of bovine serum albumin on nanosized magnetic particles. J Colloid Interface Sci 2004; 271(2): 277–283.
94. Mehta RV, Upadhyay RV, Charles SW, Ramchand CN. Direct binding of protein to magnetic particles. Biotechnol Tech 1997; 11(7): 493–496.
95. Kresse M, Wagner S, Pfefferer D, Lawaczeck R, Elste V, Semmler W. Targeting of ultrasmall superparamagnetic iron oxide (USPIO) particles to tumor cells *in vivo* by using transferrin receptor pathways. Magn Reson Med 1998; 40(2): 236–242.
96. Cengelli F, Maysinger D, Tschudi-Monnet F, Montet X, Corot C, Petri-Fink A, Hofmann H, Juillerat-Jeanneret L. Interaction of functionalized superparamagnetic iron oxide nanoparticles with brain structures. J Pharmacol Exp Ther 2006; 318(1): 108–116.
97. Zhao M, Beauregard DA, Loizou L, Davletov B, Brindle KM. Non-invasive detection of apoptosis using magnetic resonance imaging and a targeted contrast agent. Nat Med 2001; 7(11): 1241–1244.
98. Weissleder R, Lee AS, Fischman AJ, Reimer P, Shen T, Wilkinson R, Callahan RJ, Brady TJ. Polyclonal human immunoglobulin G labeled with polymeric iron oxide: antibody MR imaging. Radiology 1991; 181(1): 245–249.
99. Toma A, Otsuji E, Kuriu Y, Okamoto K, Ichikawa D, Hagiwara A, Ito H, Nishimura T, Yamagishi H. Monoclonal antibody A7-superparamagnetic iron oxide as contrast agent of MR imaging of rectal carcinoma. Br J Cancer 2005; 93(1): 131–136.
100. Li M, Xu H, Zuo J, Ji A, He B, Pang Y, Huang J, Niu R. Preparation of dextran immunological magnetic nanoparticles and their application to combined targeting carrier. Sci China B: Chem 1996; 39(6): 577–584.
101. Remsen LG, McCormick CI, Roman-Goldstein S, Nilaver G, Weissleder R, Bogdanov A, Hellström KE, Hellström I, Kroll RA, Neuwelt EA. MR of carcinoma-specific monoclonal antibody conjugated to monocrystalline iron oxide nanoparticles: the potential for noninvasive diagnosis. Am J Neuroradiol 1996; 17(3): 411–418.
102. Funovics MA, Kapeller B, Hoeller C, Su HS, Kunstfeld R, Puig S, Macfelda K. MR imaging of the her2/neu and 9.2.27 tumor antigens using immunospecific contrast agents. Magn Reson Imaging 2004; 22(6): 843–850.
103. Sonvico F, Mornet S, Vasseur S, Dubernet C, Jaillard D, Degrouard J, Hoebeke J, Duguet E, Colombo P, Couvreur P. Folate-conjugated iron oxide nanoparticles for solid tumor targeting as potential specific magnetic hyperthermia mediators: synthesis, physicochemical characterization, and in vitro experiments. Bioconjugate Chem 2005; 16(5): 1181–1188.
104. Zhang Y, Zhang J. Surface modification of monodisperse magnetite nanoparticles for improved intracellular uptake to breast cancer cells. J Colloid Interface Sci 2005; 283(2): 352–357.
105. Josephson L, Tung CH, Moore A, Weissleder R. High-efficiency intracellular magnetic labeling with novel superparamagnetic-tat peptide conjugates. Bioconjugate Chem 1999; 10(2): 186–191.
106. Hogemann D, Josephson L, Weissleder R, Basilion JP. Improvement of MRI probes to allow efficient detection of gene expression. Bioconjugate Chem 2000; 11(6): 941–946.
107. Högemann-Savellano D, Bost E, Blondet C, Sato F, Abe T, Josephson L, Weissleder R, Gaudet J, Sgroi D, Peters PJ, Basilion JP. The transferrin receptor: a potential molecular imaging marker for human cancer. Neoplasia 2003; 5(6): 495–506.
108. Won Kang H, Josephson L, Petrovsky A, Weissleder R, Bogdanov A Jr. Magnetic resonance imaging of inducible E-selectin expression in human endothelial cell culture. Bioconjugate Chem 2002; 13(1): 122–127.
109. Sun C, Sze R, Zhang M. Folic acid-PEG conjugated superparamagnetic nanoparticles for targeted cellular uptake and detection by MRI. J Biomed Mater Res A 2006; 78(3): 550–557.
110. Josephson L, Kircher MF, Mahmood U, Tang Y, Weissleder R. Near-infrared fluorescent nanoparticles as combined MR/optical imaging probes. Bioconjugate Chem 2002; 13(3): 554–560.
111. Dodd CH, Hsu HC, Chu WJ, Yang P, Zhang HG, Mountz JD Jr, Zinn K, Forder J, Josephson L, Weissleder R, Mountz JM, Mountz JD. Normal T-cell response and in vivo magnetic resonance imaging of T cells loaded with HIV transactivator-peptide-derived superparamagnetic nanoparticles. J Immunol Methods 2001; 256(1/2): 89–105.
112. Papisov MI, Bogdanov A Jr, Schaffer B, Nossiff N, Shen T, Weissleder R, Brady TJ. Colloidal magnetic resonance contrast agents: effect of particle surface on biodistribution. J Magn Magn Mater 1993; 122(1–3): 383–386.
113. Koch AM, Reynolds F, Merkle HP, Weissleder R, Josephson L. Transport of surface-modified nanoparticles through cell monolayers. ChemBioChem 2005; 6(2): 337–345.
114. Funovics M, Montet X, Reynolds F, Weissleder R, Josephson L. Nanoparticles for the optical imaging of tumor E-selectin. Neoplasia 2005; 7(10): 904–911.
115. Kircher MF, Josephson L, Weissleder R. Ratio imaging of enzyme activity using dual wavelength optical reporters. Mol Imaging 2002; 1 (2): 89–95.
116. Kircher MF, Weissleder R, Josephson L. A dual fluorochrome probe for imaging proteases. Bioconjugate Chem 2004; 15(2): 242–248.
117. Moore A, Medarova Z, Potthast A, Dai G. *In vivo* targeting of underglycosylated MUC-1 tumor antigen using a multimodal imaging probe. Cancer Res 2004; 64(5): 1821–1827.
118. Högemann D, Ntziachristos V, Josephson L, Weissleder R. High throughput magnetic resonance imaging for evaluating targeted nanoparticle probes. Bioconjugate Chem 2002; 13(1): 116–121.
119. Tsourkas A, Shinde-Patil VR, Kelly KA, Patel P, Wolley A, Allport JR, Weissleder R. In vivo imaging of activated endothelium using an anti-VCAM-1 magnetooptical probe. Bioconjugate Chem 2005; 16(3): 576–581.
120. Montet X, Funovics M, Montet-Abou K, Weissleder R, Josephson L. Multivalent effects of RGD peptides obtained by nanoparticle display. J Med Chem 2006; 49(20): 6087–6093.
121. Montet X, Montet-Abou K, Reynolds F, Weissleder R, Josephson L. Nanoparticle imaging of integrins on tumor cells. Neoplasia 2006; 8(3): 214–222.
122. Kelly KA, Allport JR, Tsourkas A, Shinde-Patil VR, Josephson L, Weissleder R. Detection of vascular adhesion molecule-1 expression using a novel multimodal nanoparticle. Circ Res 2005; 96(3): 327–336.
123. Weissleder R, Kelly K, Sun EY, Shtatland T, Josephson L. Cell-specific targeting of nanoparticles by multivalent attachment of small molecules. Nat Biotechnol 2005; 23(11): 1418–1423.
124. Kircher MF, Mahmood U, King RS, Weissleder R, Josephson L. A multimodal nanoparticle for preoperative magnetic resonance imaging and intraoperative optical brain tumor delineation. Cancer Res 2003; 63(23): 8122–8125.
125. Halbreich A, Roger J, Pons JN, Da Silva MdF, Hasmonay E, Roudier M, Boynard M, Sestier C, Amri A, Geldwerth D, Fertil B, Bacri JC, Sabolovic D. Magnetic maghemite nanoparticles: their preparation, properties, and application in cell sorting and characterization of cellular membranes in vitro. Scientific and Clinical Applications of Magnetic Carriers. Plenum: New York, 1997; 399–417.
126. Jun YW, Huh YM, Choi JS, Lee JH, Song HT, Kim S, Yoon S, Kim KS, Shin JS, Suh JS, Cheon J. Nanoscale size effect of magnetic nanocrystals and their utilisation for cancer diagnosis via magnetic resonance imaging. J Am Chem Soc 2005; 127(16): 5732–5733.
127. Huh YM, Jun YW, Song HT, Kim S, Choi JS, Lee JH, Yoon S, Kim KS, Shin JS, Suh JS, Cheon J. In vivo magnetic resonance detection of cancer by using multifunctional magnetic nanocrystals. J Am Chem Soc 2005; 127(35): 12387–12391.

128. Halbreich A, Sabolovic D, Sestier C, Amri A, Pons JN, Roger J, Geldwerth D. Annexin V binding to mouse erythrocytes following infection with Plasmodium parasites [2]. Parasitol Today 1996; 12 (7): 292–293.
129. Sestier C, Sabolovic D, Geldwerth D, Moumaris M, Roger J, Pons JN, Halbreich A. Use of annexin V-ferrofluid to enumerate erythrocytes damaged in various pathologies or during storage in vitro. C R Acad Sci III 1995; 318(11): 1141–1146.
130. Roger J, Pons JN, Massart R, Halbreich A, Bacri JC. Some biomedical applications of ferrofluids. Eur Phys J Appl Phys 1999; 5(3): 321–325.
131. Halbreich A, Roger J, Pons JN, Geldwerth D, Da Silva MF, Roudier M, Bacri JC. Biomedical applications of maghemite ferrofluid. Biochimie 1998; 80(5/6): 379–390.
132. Whitehead RA, Chagnon MS, Groman EV, Josephson L. Magnetic particles for use in separations. US Patent 1987; 4: 695–392.
133. Bridot J-L, Stanicki D, Laurent S, Boutry S, Gossuin Y, Leclère P, Lazzaroni R, Vander Elst L, Muller RN. New carboxysilane coated iron oxide nanoparticles for non-specific cell labelling. Contrast Media Mol Imaging 2013; 8: 466–474.
134. Zhang Y, Kohler N, Zhang M. Intracellular uptake of poly(ethylene glycol) and folic acid modified magnetite nanoparticles. Mater Res Soc Proc 2001; 676: Y9.8.1–Y9.8.5.
135. Liu X, Xing J, Guan Y, Shan G, Liu H. Synthesis of amino-silane modified superparamagnetic silica supports and their use for protein immobilization. Colloids Surf A: Physicochem Eng Aspects 2004; 238(1–3): 127–131.
136. Sun EY, Josephson L, Weissleder R. 'Clickable' nanoparticles for targeted imaging. Mol Imaging 2006; 5(2): 122–128.
137. Müller-Schulte DFF, Lueken H, De Cuyper M. Neuer Ansatz für die AIDS-Therapie unter Verwendung superparamagnetischer Nanopartikel. Alma Mater Aquensis 1995; 31: 174–187.
138. Shinkai M, Suzuki M, Iijima S, Kobayashi T. Antibody-conjugated magnetoliposomes for targeting cancer cells and their application in hyperthermia. Biotechnol Applied Biochem 1995; 21(2): 125–137.
139. Sun EY, Josephson L, Weissleder R. 'Clickable' nanoparticles for targeted imaging. Mol Imaging 2006; 5(2): 122–128.
140. Domingo JC, Mercadal M, Petriz J, De Madariaga MA. Preparation of PEG-grafted immunomagnetoliosomes entrapping citrate stabilized magnetite particles and their application in CD34+ cell sorting. J Microencapsul 2001; 18(1): 41–54.
141. Ito A, Kuga Y, Honda H, Kikkawa H, Horiuchi A, Watanabe Y, Kobayashi T. Magnetite nanoparticle-loaded anti-HER2 immunoliposomes for combination of antibody therapy with hyperthermia. Cancer Lett 2004; 212(2): 167–175.
142. Ito A, Ino K, Kobayashi T, Honda H. The effect of RGD peptide-conjugated magnetite cationic liposomes on cell growth and cell sheet harvesting. Biomaterials 2005; 26(31): 6185–6193.
143. Hodenius M, De Cuyper M, Desender L, Müller-Schulte D, Steigel A, Lueken H. Biotinylated Stealth® magnetoliposomes. Chem Phys Lipids 2002; 120(1/2): 75–85.
144. Nitin N, LaConte LEW, Zurkiya O, Hu X, Bao G. Functionalization and peptide-based delivery of magnetic nanoparticles as an intracellular MRI contrast agent. J Biol Inorg Chem 2004; 9(6): 706–712.
145. Nasongkla N, Bey E, Ren J, Ai H, Khemtong C, Guthi JS, Chin SF, Sherry AD, Boothman DA, Gao J. Multifunctional polymeric micelles as cancer-targeted, MRI-ultrasensitive drug delivery systems. Nano Lett 2006; 6(11): 2427–2430.
146. Rennen HJ, Boerman OC, Oyen WJ, Corstens FH. Imaging infection/inflammation in the new millennium. Eur J Nucl Med 2001; 28(2): 241–252.
147. Kooi M, Cappendijk V, Cleutjens K, Kessels A, Kitslaar P, Borgers M, Frederik P, Daemen M, Van Engelshoven J. Accumulation of ultrasmall superparamagnetic particles of iron oxide in human atherosclerotic plaques can be detected by in vivo magnetic resonance imaging. Circulation 2003; 107(19): 2453–2458.
148. Beckmann N, Cannet C, Fringeli-Tanner M, Baumann D, Pally C, Bruns C, Zerwes HG, Andriambeloson E, Bigaud M. Macrophage labeling by SPIO as an early marker of allograft chronic rejection in a rat model of kidney transplantation. Magn Reson Med 2003; 49(3): 459–467.
149. Barber PA, Foniok T, Kirk D, Buchan AM, Laurent S, Boutry S, Muller RN, Hoyte L, Tomanek B, Tuor UI. MR molecular imaging of early endothelial activation in focal ischemia. Ann Neurol 2004; 56(1): 116–120.
150. Tanaka Y. The role of chemokines and adhesion molecules in the pathogenesis of rheumatoid arthritis. Drugs Today (Barc) 2001; 37(7): 477–484.
151. Khatib A-M, Kontogiannea M, Fallavollita L, Jamison B, Meterissian S, Brodt P. Rapid induction of cytokine and E-selectin expression in the liver in response to metastatic tumor cells. Cancer Res 1999; 59(6): 1356–1361.
152. Menger MD, Vollmar B. Role of microcirculation in transplantation. Microcirculation 2000; 7(5): 291–306.
153. Dousset V, Delalande C, Ballarino L, Quesson B, Seilhan D, Coussemacq M, Thiaudiére E, Brochet B, Canioni P, Caillé JM. In vivo macrophage activity imaging in the central nervous system detected by magnetic resonance. Magn Reson Med 1999; 41(2): 329–333.
154. Dousset V, Gomez C, Petry KG, Delalande C, Caille J-M. Dose and scanning delay using USPIO for central nervous system macrophage imaging. Magn Reson Mater Phys Biol Med 1999; 8(3): 185–189.
155. Fleige G, Nolte C, Synowitz M, Seeberger F, Kettenmann H, Zimmer C. Magnetic labeling of activated microglia in experimental gliomas. Neoplasia 2001; 3(6): 489.
156. Rausch M, Hiestand P, Baumann D, Cannet C, Rudin M. MRI-based monitoring of inflammation and tissue damage in acute and chronic relapsing EAE. Magn Reson Med 2003; 50(2): 309–314.
157. Ruehm SG, Corot C, Vogt P, Kolb S, Debatin JF. Magnetic resonance imaging of atherosclerotic plaque with ultrasmall superparamagnetic particles of iron oxide in hyperlipidemic rabbits. Circulation 2001; 103(3): 415–422.
158. Kang HW, Josephson L, Petrovsky A, Weissleder R, Bogdanov A. Magnetic resonance imaging of inducible E-selectin expression in human endothelial cell culture. Bioconjugate Chem 2002; 13(1): 122–127.
159. Alsaid H, De Souza G, Bourdillon M-C, Chaubet F, Sulaiman A, Desbleds-Mansard C, Chaabane L, Zahir C, Lancelot E, Rousseaux O. Biomimetic MRI contrast agent for imaging of inflammation in atherosclerotic plaque of $ApoE^{-/-}$ mice: a pilot study. Invest Radiol 2009; 44(3): 151–158.
160. Winter PM, Caruthers SD, Kassner A, Harris TD, Chinen LK, Allen JS, Lacy EK, Zhang H, Robertson JD, Wickline SA. Molecular imaging of angiogenesis in nascent Vx-2 rabbit tumors using a novel $\alpha_v\beta_3$-targeted nanoparticle and 1.5 tesla magnetic resonance imaging. Cancer Res 2003; 63(18): 5838–5843.
161. Albelda SM, Buck CA. Integrins and other cell adhesion molecules. FASEB J 1990; 4(11): 2868–2880.
162. Foxall C, Watson SR, Dowbenko D, Fennie C, Lasky LA, Kiso M, Hasegawa A, Asa D, Brandley BK. The three members of the selectin receptor family recognize a common carbohydrate epitope, the sialyl $Lewis^x$ oligosaccharide. J Cell Biol 1992; 117(4): 895–902.
163. Vestweber D, Blanks JE. Mechanisms that regulate the function of the selectins and their ligands. Physiol Rev 1999; 79(1): 181–213.
164. Boutry S, Laurent S, Elst LV, Muller RN. Specific E-selectin targeting with a superparamagnetic MRI contrast agent. Contrast Media Mol Imaging 2006; 1(1): 15–22.
165. Laurent S, Vander Elst L, Fu Y, Muller RN. Synthesis and physicochemical characterization of Gd-DTPA-B (sLex) A, a new MRI contrast agent targeted to inflammation. Bioconjugate Chem 2004; 15(1): 99–103.
166. Sibson NR, Blamire AM, Bernades-Silva M, Laurent S, Boutry S, Muller RN, Styles P, Anthony DC. MRI detection of early endothelial activation in brain inflammation. Magn Reson Med 2004; 51(2): 248–252.
167. Boutry S, Burtea C, Laurent S, Toubeau G, Vander Elst L, Muller RN. Magnetic resonance imaging of inflammation with a specific selectin-targeted contrast agent. Magn Reson Med 2005; 53(4): 800–807.
168. Serda RE, Adolphi NL, Bisoffi M, Sillerud LO. Targeting and cellular trafficking of magnetic nanoparticles for prostate cancer imaging. Mol Imaging 2007; 6(4): 277–288.
169. Kou G, Wang S, Cheng C, Gao J, Li B, Wang H, Qian W, Hou S, Zhang D, Dai J, Gu H, Guo Y. Development of SM5-1-conjugated ultrasmall superparamagnetic iron oxide nanoparticles for hepatoma detection. Biochem Biophys Res Commun 2008; 374(2): 192–197.
170. Chen TJ, Cheng TH, Chen CY, Hsu SC, Cheng TL, Liu GC, Wang YM. Targeted Herceptin–dextran iron oxide nanoparticles for noninvasive imaging of HER2/neu receptors using MRI. J Biol Inorg Chem 2009; 14(2): 253–260.
171. Yang H-M, Park CW, Woo M-A, Kim MI, Jo YM, Park HG, Kim J-D. HER2/neu antibody conjugated poly(amino acid)-coated iron oxide

nanoparticles for breast cancer MR imaging. Biomacromolecules 2010; 11(11): 2866–2872.
172. Song E-Q, Hu J, Wen C-Y, Tian Z-Q, Yu X, Zhang Z-L, Shi Y-B, Pang D-W. Fluorescent–magnetic–biotargeting multifunctional nanobioprobes for detecting and isolating multiple types of tumor cells. ACS Nano 2011; 5(2): 761–770.
173. Jain RK. Transport of molecules in the tumor interstitium: a review. Cancer Res 1987; 47(12): 3039–3051.
174. McNeil SE. Nanotechnology for the biologist. J Leukoc Biol 2005; 78(3): 585–594.
175. Yang L, Mao H, Wang YA, Cao Z, Peng X, Wang X, Duan H, Ni C, Yuan Q, Adams G, Smith MQ, Wood WC, Gao X, Nie S. Single chain epidermal growth factor receptor antibody conjugated nanoparticles for in vivo tumor targeting and imaging. Small 2009; 5(2): 235–243.
176. Yang L, Mao H, Cao Z, Wang YA, Peng X, Wang X, Sajja HK, Wang L, Duan H, Ni C, Staley CA, Wood WC, Gao X, Nie S. Molecular imaging of pancreatic cancer in an animal model using targeted multifunctional nanoparticles. Gastroenterology 2009; 136(5): 1514–1525.
177. Chatzistamou L, Schally AV, Nagy A, Armatis P, Szepeshazi K, Halmos G. Effective treatment of metastatic MDA-MB-435 human estrogen-independent breast carcinomas with a targeted cytotoxic analogue of luteinizing hormone-releasing hormone AN-207. Clin Cancer Res 2000; 6(10): 4158–4165.
178. Leuschner C, Kumar CS, Hansel W, Soboyejo W, Zhou J, Hormes J. LHRH-conjugated magnetic iron oxide nanoparticles for detection of breast cancer metastases. Breast Cancer Res Treat 2006; 99(2): 163–176.
179. Ichikawa T, Hogemann D, Saeki Y, Tyminski E, Terada K, Weissleder R, Chiocca EA, Basilion JP. MRI of transgene expression: correlation to therapeutic gene expression. Neoplasia 2002; 4(6): 523–530.
180. Moore A, Basilion JP, Chiocca EA, Weissleder R. Measuring transferrin receptor gene expression by NMR imaging. Biochim Biophys Acta 1998; 24(3): 239–249.
181. Weissleder R, Moore A, Mahmood U, Bhorade R, Benveniste H, Chiocca EA, Basilion JP. *In vivo* magnetic resonance imaging of transgene expression. Nat Med 2000; 6(3): 351–355.
182. Low PS, Henne WA, Doorneweerd DD. Discovery and development of folic-acid-based receptor targeting for imaging and therapy of cancer and inflammatory diseases. Acc Chem Res 2008; 41(1): 120–129.
183. Choi H, Choi SR, Zhou R, Kung HF, Chen IW. Iron oxide nanoparticles as magnetic resonance contrast agent for tumor imaging via folate receptor-targeted delivery. Acad Radiol 2004; 11(9): 996–1004.
184. Sun C, Sze R, Zhang M. Folic acid-PEG conjugated superparamagnetic nanoparticles for targeted cellular uptake and detection by MRI. J Biomed Mater Res A 2006; 78(3): 550–557.
185. Chen H, Gu Y, Hub Y, Qian Z. Characterization of pH- and temperature-sensitive hydrogel nanoparticles for controlled drug release. Parenter Drug Assoc J Pharm Sci Technol 2007; 61(4): 303–313.
186. Shen TT, Bogdanov A Jr, Bogdanova A, Poss K, Brady TJ, Weissleder R. Magnetically labeled secretin retains receptor affinity to pancreas acinar cells. Bioconjugate Chem 1996; 7(3): 311–316.
187. Sunderland CJ, Steiert M, Talmadge JE, Derfus AM, Barry SE. Targeted nanoparticles for detecting and treating cancer. Drug Dev Res 2006; 67(1): 70–93.
188. Zhang C, Jugold M, Woenne EC, Lammers T, Morgenstern B, Mueller MM, Zentgraf H, Bock M, Eisenhut M, Semmler W, Kiessling F. Specific targeting of tumor angiogenesis by RGD-conjugated ultrasmall superparamagnetic iron oxide particles using a clinical 1.5-T magnetic resonance scanner. Cancer Res 2007; 67(4): 1555–1562.
189. Liu C, Liu DB, Long GX, Wang JF, Mei Q, Hu GY, Qiu H, Hu GQ. Specific targeting of angiogenesis in lung cancer with RGD-conjugated ultrasmall superparamagnetic iron oxide particles using a 4.7T magnetic resonance scanner. Chin Med J 2013; 126(12): 2242–2247.
190. Burtea C, Laurent S, Murariu O, Rattat D, Toubeau G, Verbruggen A, Vansthertem D, Vander Elst L, Muller RN. Molecular imaging of alpha v beta3 integrin expression in atherosclerotic plaques with a mimetic of RGD peptide grafted to Gd-DTPA. Cardiovasc Res 2008; 78(1): 148–157.
191. Rerat V, Laurent S, Burtea C, Driesschaert B, Pourcelle V, Vander Elst L, Muller RN, Marchand-Brynaert J. Ultrasmall particle of iron oxide–RGD peptidomimetic conjugate: synthesis and characterisation. Bioorganic Med Chem Lett 2010; 20(6): 1861–1865.
192. Xie J, Chen K, Lee HY, Xu C, Hsu AR, Peng S, Chen X, Sun S. Ultrasmall c(RGDyK)-coated Fe_3O_4 nanoparticles and their specific targeting to integrin alpha(v)beta3-rich tumor cells. J Am Chem Soc 2008; 130(24): 7542–7543.
193. Bamrungsap S, Chen T, Shukoor MI, Chen Z, Sefah K, Chen Y, Tan W. Pattern recognition of cancer cells using aptamer-conjugated magnetic nanoparticles. ACS Nano 2012; 6(5): 3974–3981.
194. Medley CD, Bamrungsap S, Tan W, Smith JE. Aptamer-conjugated nanoparticles for cancer cell detection. Anal Chem 2011; 83(3): 727–734.
195. Smith JE, Medley CD, Tang Z, Shangguan D, Lofton C, Tan W. Aptamer-conjugated nanoparticles for the collection and detection of multiple cancer cells. Anal Chem 2007; 79(8): 3075–3082.
196. Yu MK, Kim D, Lee IH, So JS, Jeong YY, Jon S. Image-guided prostate cancer therapy using aptamer-functionalized thermally cross-linked superparamagnetic iron oxide nanoparticles. Small 2011; 7(15): 2241–2249.
197. Wang AZ, Bagalkot V, Vasilliou CC, Gu F, Alexis F, Zhang L, Shaikh M, Yuet K, Cima MJ, Langer R, Kantoff PW, Bander NH, Jon S, Farokhzad OC. Superparamagnetic iron oxide nanoparticle–aptamer bioconjugates for combined prostate cancer imaging and therapy. ChemMedChem 2008; 3(9): 1311–1315.
198. Yigit MV, Mazumdar D, Kim H-K, Lee JH, Odintsov B, Lu Y. Smart 'turn-on' magnetic resonance contrast agents based on aptamer-functionalized superparamagnetic iron oxide nanoparticles. ChemBioChem 2007; 8(14): 1675–1678.
199. Yigit MV, Mazumdar D, Lu Y. MRI Detection of thrombin with aptamer functionalized superparamagnetic iron oxide nanoparticles. Bioconjugate Chem 2008; 19(2): 412–417.
200. Reddy LH, Couvreur P. Nanotechnology for therapy and imaging of liver diseases. J Hepatol 2011; 55(6): 1461–1466.
201. Bataller R, Brenner DA. Liver fibrosis. J Clin Invest 2005; 115(2): 209–218.
202. Faria SC, Ganesan K, Mwangi I, Shiehmorteza M, Viamonte B, Mazhar S, Peterson M, Kono Y, Santillan C, Casola G, Sirlin CB. MR imaging of liver fibrosis: current state of the art. Radiographics 2009; 29(6): 1615–1635.
203. Rosen JE, Chan L, Shieh D-B, Gu FX. Iron oxide nanoparticles for targeted cancer imaging and diagnostics. Nanomed Nanotechnol Biol Med 2012; 8(3): 275–290.
204. Qiao R, Yang C, Gao M. Superparamagnetic iron oxide nanoparticles: from preparations to in vivo MRI applications. J Mater Chem 2009; 19(35): 6274–6293.
205. Gandhi SN, Brown MA, Wong JG, Aguirre DA, Sirlin CB. MR contrast agents for liver imaging: what, when, how. Radiographics 2006; 26(6): 1621–1636.
206. Ma HL, Xu YF, Qi XR, Maitani Y, Nagai T. Superparamagnetic iron oxide nanoparticles stabilized by alginate: pharmacokinetics, tissue distribution, and applications in detecting liver cancers. Int J Pharm 2008; 354(1/2): 217–226.
207. Clement O, Frija G, Chambon C, Schouman-Clayes E, Mosnier JF, Poupon MF, Balkau B. Liver tumors in cirrhosis: experimental study with SPIO-enhanced MR imaging. Radiology 1991; 180(1): 31–36.
208. Tanimoto A, Kuribayashi S. Application of superparamagnetic iron oxide to imaging of hepatocellular carcinoma. Eur J Radiol 2006; 58(2): 200–216.
209. Aguirre DA, Behling CA, Alpert E, Hassanein TI, Sirlin CB. Liver fibrosis: noninvasive diagnosis with double contrast material-enhanced MR imaging. Radiology 2006; 239(2): 425–437.
210. Wang YX, Xuan S, Port M, Idee JM. Recent advances in superparamagnetic iron oxide nanoparticles for cellular imaging and targeted therapy research. Curr Pharm Des 2013: 6575–6593.
211. Zhang H, Ma Y, Sun XL. Recent developments in carbohydrate-decorated targeted drug/gene delivery. Med Res Rev 2010; 30(2): 270–289.
212. Lee C-M, Jeong H-J, Kim E-M, Kim DW, Lim ST, Kim HT, Park I-K, Jeong YY, Kim JW, Sohn M-H. Superparamagnetic iron oxide nanoparticles as a dual imaging probe for targeting hepatocytes in vivo. Magn Reson Med 2009; 62(6): 1440–1446.
213. Zhao M, Beauregard DA, Loizou L, Davletov B, Brindle KM. Non-invasive detection of apoptosis using magnetic resonance imaging and a targeted contrast agent. Nat Med 2001; 7(11): 1241–1244.
214. Radermacher KA, Boutry S, Laurent S, Elst LV, Mahieu I, Bouzin C, Magat J, Gregoire V, Feron O, Muller RN, Jordan BF, Gallez B. Iron oxide particles covered with hexapeptides targeted at

phosphatidylserine as MR biomarkers of tumor cell death. Contrast Media Mol Imaging 2010; 5(5): 258–267.
215. Vu-Quang H, Muthiah M, Lee HJ, Kim Y-K, Rhee JH, Lee J-H, Cho C-S, Choi Y-J, Jeong YY, Park I-K. Immune cell-specific delivery of beta-glucan-coated iron oxide nanoparticles for diagnosing liver metastasis by MR imaging. Carbohydr Polym 2012; 87(2): 1159–1168.
216. Kolosnjaj-Tabi J, Wilhelm C, Clement O, Gazeau F. Cell labeling with magnetic nanoparticles: opportunity for magnetic cell imaging and cell manipulation. J Nanobiotechnol 2013; 11(Suppl 1): S7.
217. Luciani A, Parouchev A, Smirnov P, Braga G, Wilhelm C, Gazeau F, Boudechiche L, L'Hermine-Coulomb A, Dagher I, Franco D, Rahmouni A, Hadchouel M, Weber A, Clement O. In vivo imaging of transplanted hepatocytes with a 1.5-T clinical MRI system – initial experience in mice. Eur Radiol 2008; 18(1): 59–69.
218. Maccioni F, Colaiacomo MC, Parlanti S. Ulcerative colitis: value of MR imaging. Abdom Imaging 2005; 30(5): 584–592.
219. Wang YX, Hussain SM, Krestin GP. Superparamagnetic iron oxide contrast agents: physicochemical characteristics and applications in MR imaging. Eur Radiol 2001; 11(11): 2319–2331.
220. Hahn PF, Stark DD, Lewis JM, Saini S, Elizondo G, Weissleder R, Fretz CJ, Ferrucci JT. First clinical trial of a new superparamagnetic iron oxide for use as an oral gastrointestinal contrast agent in MR imaging. Radiology 1990; 175(3): 695–700.
221. Wang Y-XJ. Superparamagnetic iron oxide based MRI contrast agents: current status of clinical application. Quant Imaging Med Surg 2011; 1(1): 35–40.
222. D'Arienzo A, Scaglione G, Vicinanza G, Manguso F, Bennato R, Belfiore G, Imbriaco M, Mazzacca G. Magnetic resonance imaging with ferumoxil, a negative superparamagnetic oral contrast agent, in the evaluation of ulcerative colitis. Am J Gastroenterol 2000; 95(3): 720–724.
223. Xiao B, Merlin D. Oral colon-specific therapeutic approaches toward treatment of inflammatory bowel disease. Expert Opin Drug Deliv 2012; 9(11): 1393–1407.
224. Crater JS, Carrier RL. Barrier properties of gastrointestinal mucus to nanoparticle transport. Macromol Biosci 2010; 10(12): 1473–1483.
225. Kenzaoui BH, Vila MR, Miquel JM, Cengelli F, Juillerat-Jeanneret L. Evaluation of uptake and transport of cationic and anionic ultrasmall iron oxide nanoparticles by human colon cells. Int J Nanomedicine 2012; 7: 1275–1286.
226. Elias A, Tsourkas A. Imaging circulating cells and lymphoid tissues with iron oxide nanoparticles. Hematology 2009; 2009(1): 720–726.
227. Jahan N, Narayanan P, Rockall A. Magnetic resonance lymphography in gynaecological malignancies. Cancer Imaging 2010; 10: 85–96.
228. Koh DM, Cook GJ, Husband JE. New horizons in oncologic imaging. N Engl J Med 2003; 348(25): 2487–2488.
229. Benedetti-Panici P, Maneschi F, Scambia G, Greggi S, Cutillo G, D'Andrea G, Rabitti C, Coronetta F, Capelli A, Mancuso S. Lymphatic spread of cervical cancer: an anatomical and pathological study based on 225 radical hysterectomies with systematic pelvic and aortic lymphadenectomy. Gynecol Oncol 1996; 62(1): 19–24.
230. Hövels AM, Heesakkers RAM, Adang EM, Jager GJ, Strum S, Hoogeveen YL, Severens JL, Barentsz JO. The diagnostic accuracy of CT and MRI in the staging of pelvic lymph nodes in patients with prostate cancer: a meta-analysis. Clin Radiol 2008; 63(4): 387–395.
231. Islam T, Harisinghani MG. Overview of nanoparticle use in cancer imaging. Cancer Biomark 2009; 5(2): 61–67.
232. Weissleder R, Bogdanov A, Neuwelt EA, Papisov M. Long-circulating iron oxides for MR imaging. Adv Drug Deliv Rev 1995; 16(2–3): 321–334.
233. Bellin M-F, Beigelman C, Precetti-Morel S. Iron oxide-enhanced MR lymphography: initial experience. Eur J Radiol 2000; 34(3): 257–264.
234. Schroeder A, Heller DA, Winslow MM, Dahlman JE, Pratt GW, Langer R, Jacks T, Anderson DG. Treating metastatic cancer with nanotechnology. Nat Rev Cancer 2012; 12(1): 39–50.
235. Raynal I, Prigent P, Peyramaure S, Najid A, Rebuzzi C, Corot C. Macrophage Endocytosis of Superparamagnetic Iron Oxide Nanoparticles: Mechanisms and Comparison of Ferumoxides and Ferumoxtran-10. Invest. Radiol 2004; 39(1): 56–63.
236. Ferrucci JT, Stark DD. Iron oxide-enhanced MR imaging of the liver and spleen: review of the first 5 years. Am J Roentgenol 1990; 155(5): 943–950.
237. Daldrup-Link H, Rummeny E, Ihssen B, Kienast J, Link T. Iron-oxide-enhanced MR imaging of bone marrow in patients with non-Hodgkin's lymphoma: differentiation between tumor infiltration and hypercellular bone marrow. Eur Radiol 2002; 12(6): 1557–1566.
238. Jung CW, Rogers JM, Groman EV. Lymphatic mapping and sentinel node location with magnetite nanoparticles. J Magn Magn Mater 1999; 194(1–3): 210–216.
239. Harisinghani MG, Barentsz J, Hahn PF, Deserno WM, Tabatabaei S, van de Kaa CH, de la Rosette J, Weissleder R. Noninvasive detection of clinically occult lymph-node metastases in prostate cancer. N Engl J Med 2003; 348(25): 2491–2499.
240. Deserno WM, Harisinghani MG, Taupitz M, Jager GJ, Witjes JA, Mulders PF. Hulsbergen van de Kaa CA, Kaufmann D, Barentsz JO. Urinary bladder cancer: preoperative nodal staging with ferumoxtran-10-enhanced MR imaging. Radiology 2004; 233(2): 449–456.
241. Harisinghani MG, Saksena M, Ross RW, Tabatabaei S, Dahl D, McDougal S, Weissleder R. A pilot study of lymphotrophic nanoparticle-enhanced magnetic resonance imaging technique in early stage testicular cancer: a new method for noninvasive lymph node evaluation. Urology 2005; 66(5): 1066–1071.
242. Tabatabaei S, Harisinghani M, McDougal WS. Regional lymph node staging using lymphotropic nanoparticle enhanced magnetic resonance imaging with ferumoxtran-10 in patients with penile cancer. J Urol 2005; 174(3): 923–927.
243. Nishimura H, Tanigawa N, Hiramatsu M, Tatsumi Y, Matsuki M, Narabayashi I. Preoperative esophageal cancer staging: magnetic resonance imaging of lymph node with ferumoxtran-10, an ultrasmall superparamagnetic iron oxide. J Am Coll Surg 2006; 202(4): 604–611.
244. Koh D-M, Brown G, Temple L, Raja A, Toomey P, Bett N, Norman AR, Husband JE. Rectal cancer: mesorectal lymph nodes at MR imaging with USPIO versus histopathologic findings – initial observations. Radiology 2004; 231(1): 91–99.
245. Rockall AG, Sohaib SA, Harisinghani MG, Babar SA, Singh N, Jeyarajah AR, Oram DH, Jacobs IJ, Shepherd JH, Reznek RH. Diagnostic performance of nanoparticle-enhanced magnetic resonance imaging in the diagnosis of lymph node metastases in patients with endometrial and cervical cancer. J Clin Oncol 2005; 23(12): 2813–2821.
246. Shapiro EM, Medford-Davis LN, Fahmy TM, Dunbar CE, Koretsky AP. Antibody-mediated cell labeling of peripheral T cells with micron-sized iron oxide particles (MPIOs) allows single cell detection by MRI. Contrast Media Mol Imaging 2007; 2(3): 147–153.
247. Arbab AS, Bashaw LA, Miller BR, Jordan EK, Bulte JWM, Frank JA. Intracytoplasmic tagging of cells with ferumoxides and transfection agent for cellular magnetic resonance imaging after cell transplantation: methods and techniques. Transplantation 2003; 76(7): 1123–1130.
248. de Vries IJ, Lesterhuis WJ, Barentsz JO, Verdijk P, van Krieken JH, Boerman OC, Oyen WJ, Bonenkamp JJ, Boezeman JB, Adema GJ, Bulte JW, Scheenen TW, Punt CJ, Heerschap A, Figdor CG. Magnetic resonance tracking of dendritic cells in melanoma patients for monitoring of cellular therapy. Nat Biotechnol 2005; 23(11): 1407–1413.
249. Kobukai S, Baheza R, Cobb JG, Virostko J, Xie J, Gillman A, Koktysh D, Kerns D, Does M, Gore JC, Pham W. Magnetic nanoparticles for imaging dendritic cells. Magn Reson Med 2010; 63(5): 1383–1390.
250. Karagulle-Kendi AT, Truwit C. Neuroimaging of central nervous system infections. Handbook of Clinical Neurology Vol 96. Elsevier: Amsterdam, 2010; 239–255.
251. Krol S, Macrez R, Docagne F, Defer G, Laurent S, Rahman M, Hajipour MJ, Kehoe PG, Mahmoudi M. Therapeutic benefits from nanoparticles: the potential significance of nanoscience in diseases with compromise to the blood brain barrier. Chem Rev 2012; 113(3): 1877–1903.
252. Petry K, Boiziau C, Dousset V, Brochet B. Magnetic resonance imaging of human brain macrophage infiltration. Neurotherapeutics 2007; 4(3): 434–442.
253. Dousset V, Brochet B, Deloire MSA, Lagoarde L, Barroso B, Caille J-M, Petry KG. MR imaging of relapsing multiple sclerosis patients using ultra-small-particle iron oxide and compared with gadolinium. Am J Neuroradiol 2006; 27(5): 1000–1005.
254. Heyn C, Ronald JA, Mackenzie LT, MacDonald IC, Chambers AF, Rutt BK, Foster PJ. In vivo magnetic resonance imaging of single cells in

mouse brain with optical validation. Magn Reson Med 2006; 55(1): 23–29.
255. Grossman RI, Braffman BH, Brorson JR, Goldberg HI, Silberberg DH, Gonzalez-Scarano F. Multiple sclerosis: serial study of gadolinium-enhanced MR imaging. Radiology 1988; 169(1): 117–122.
256. Dousset V, Delalande C, Ballarino L, Quesson B, Seilhan D, Coussemacq M, Thiaudiere E, Brochet B, Canioni P, Caille JM. In vivo macrophage activity imaging in the central nervous system detected by magnetic resonance. Magn Reson Med 1999; 41(2): 329–333.
257. Dousset V, Gomez C, Petry K, Delalande C, Caille J-M. Dose and scanning delay using USPIO for central nervous system macrophage imaging. Magn Reson Mater Phys Biol Med 1999; 8(3): 185–189.
258. Kenzaoui BH, Bernasconi CC, Hofmann H, Juillerat-Jeanneret L. Evaluation of uptake and transport of ultrasmall superparamagnetic iron oxide nanoparticles by human brain-derived endothelial cells. Nanomedicine (Lond) 2012; 7(1): 39–53.
259. Dan M, Cochran DB, Yokel RA, Dziubla TD. Binding, transcytosis and biodistribution of anti-PECAM-1 iron oxide nanoparticles for brain-targeted delivery. PLoS One 2013; 8(11): e81051.
260. Floris S, Blezer ELA, Schreibelt G, Döpp E, van der Pol SMA, Schadee-Eestermans IL, Nicolay K, Dijkstra CD, de Vries HE. Blood–brain barrier permeability and monocyte infiltration in experimental allergic encephalomyelitis: a quantitative MRI study. Brain 2004; 127(3): 616–627.
261. Dousset V, Ballarino L, Delalande C, Coussemacq M, Canioni P, Petry KG, Caillé J-M. Comparison of ultrasmall particles of iron oxide (USPIO)-enhanced T2-weighted, conventional T2-weighted, and gadolinium-enhanced T1-weighted MR images in rats with experimental autoimmune encephalomyelitis. Am J Neuroradiol 1999; 20(2): 223–227.
262. Rausch M, Hiestand P, Foster CA, Baumann DR, Cannet C, Rudin M. Predictability of FTY720 efficacy in experimental autoimmune encephalomyelitis by in vivo macrophage tracking: clinical implications for ultrasmall superparamagnetic iron oxide-enhanced magnetic resonance imaging. J Magn Reson Imaging 2004; 20(1): 16–24.
263. Bendszus M, Stoll G. Caught in the act: *in vivo* mapping of macrophage infiltration in nerve injury by magnetic resonance imaging. J Neurosci 2003; 23(34): 10892–10896.
264. Arvin B, Neville LF, Barone FC, Feuerstein GZ. The role of inflammation and cytokines in brain injury. Neurosci Biobehav Rev 1996; 20(3): 445–452.
265. Zelivyanskaya ML, Nelson JA, Poluektova L, Uberti M, Mellon M, Gendelman HE, Boska MD. Tracking superparamagnetic iron oxide labeled monocytes in brain by high-field magnetic resonance imaging. J Neurosci Res 2003; 73(3): 284–295.
266. Rausch M, Hiestand P, Baumann D, Cannet C, Rudin M. MRI-based monitoring of inflammation and tissue damage in acute and chronic relapsing EAE. Magn Reson Med 2003; 50(2): 309–314.
267. Corot C, Petry KG, Trivedi R, Saleh A, Jonkmanns C, Le Bas J-F, Blezer E, Rausch M, Brochet B, Foster-Gareau P, Balériaux D, Gaillard S, Dousset V. Macrophage imaging in central nervous system and in carotid atherosclerotic plaque using ultrasmall superparamagnetic iron oxide in magnetic resonance imaging. Invest Radiol 2004; 39(10): 619–625.
268. Schilling M, Besselmann M, Leonhard C, Mueller M, Ringelstein EB, Kiefer R. Microglial activation precedes and predominates over macrophage infiltration in transient focal cerebral ischemia: a study in green fluorescent protein transgenic bone marrow chimeric mice. Exp Neurol 2003; 183(1): 25–33.
269. Saleh A, Schroeter M, Jonkmanns C, Hartung HP, Modder U, Jander S. *In vivo* MRI of brain inflammation in human ischaemic stroke. Brain 2004; 127(7): 1670–1677.
270. Deddens LH, Van Tilborg GA, Mulder WJ, De Vries HE, Dijkhuizen RM. Imaging neuroinflammation after stroke: current status of cellular and molecular MRI strategies. Cerebrovasc Dis 2012; 33(4): 392–402.
271. Oude Engberink RD, Blezer ELA, Hoff EI, van der Pol SMA, van der Toorn A, Dijkhuizen RM, de Vries HE. MRI of monocyte infiltration in an animal model of neuroinflammation using SPIO-labeled monocytes or free USPIO. J Cereb Blood Flow Metab 2007; 28(4): 841–851.
272. Henning EC, Ruetzler CA, Gaudinski MR, Hu TC, Latour LL, Hallenbeck JM, Warach S. Feridex preloading permits tracking of CNS-resident macrophages after transient middle cerebral artery occlusion. J Cereb Blood Flow Metab 2009; 29(7): 1229–1239.
273. Lorger M, Felding-Habermann B. Capturing changes in the brain microenvironment during initial steps of breast cancer brain metastasis. Am J Pathol 2010; 176(6): 2958–2971.
274. Lorger M. Tumor microenvironment in the brain. Cancers 2012; 4(1): 218–243.
275. Enochs WS, Harsh G, Hochberg F, Weissleder R. Improved delineation of human brain tumors on MR images using a long-circulating, superparamagnetic iron oxide agent. J Magn Reson Imaging 1999; 9(2): 228–232.
276. Neuwelt EA, Varallyay P, Bago AG, Muldoon LL, Nesbit G, Nixon R. Imaging of iron oxide nanoparticles by MR and light microscopy in patients with malignant brain tumours. Neuropathol Appl Neurobiol 2004; 30(5): 456–471.
277. Zimmer C, Weissleder R, Poss K, Bogdanova A, Wright SC Jr, Enochs WS. MR imaging of phagocytosis in experimental gliomas. Radiology 1995; 197(2): 533–538.
278. Fleige G, Nolte C, Synowitz M, Seeberger F, Kettenmann H, Zimmer C. Magnetic labeling of activated microglia in experimental gliomas. Neoplasia 2001; 3(6): 489–499.
279. Sztriha LK, O'Gorman RL, Modo M, Barker GJ, Williams SCR, Kalra L. Monitoring brain repair in stroke using advanced magnetic resonance imaging. Stroke 2012; 43(11): 3124–3131.
280. Schwartz CJ, Valente AJ, Sprague EA, Kelley JL, Cayatte AJ, Mowery J. Atherosclerosis. Potential targets for stabilization and regression. Circulation 1992; 86(6 Suppl): III117–123.
281. Corot C, Petry KG, Trivedi R, Saleh A, Jonkmanns C, Le Bas JF, Blezer E, Rausch M, Brochet B, Foster-Gareau P, Baleriaux D, Gaillard S, Dousset V. Macrophage imaging in central nervous system and in carotid atherosclerotic plaque using ultrasmall superparamagnetic iron oxide in magnetic resonance imaging. Invest Radiol 2004; 39(10): 619–625.
282. Tang TY, Muller KH, Graves MJ, Li ZY, Walsh SR, Young V, Sadat U, Howarth SP, Gillard JH. Iron oxide particles for atheroma imaging. Arteriosclerosis Thromb Vasc Biol 2009; 29(7): 1001–1008.
283. Ruehm SG, Corot C, Vogt P, Kolb S, Debatin JF. Magnetic resonance imaging of atherosclerotic plaque with ultrasmall superparamagnetic particles of iron oxide in hyperlipidemic rabbits. Circulation 2001; 103(3): 415–422.
284. Schmitz SA, Coupland SE, Gust R, Winterhalter S, Wagner S, Kresse M, Semmler W, Wolf KJ. Superparamagnetic iron oxide-enhanced MRI of atherosclerotic plaques in Watanabe hereditable hyperlipidemic rabbits. Invest Radiol 2000; 35(8): 460–471.
285. Litovsky S, Madjid M, Zarrabi A, Casscells SW, Willerson JT, Naghavi M. Superparamagnetic iron oxide-based method for quantifying recruitment of monocytes to mouse atherosclerotic lesions in vivo: enhancement by tissue necrosis factor-alpha, interleukin-1beta, and interferon-gamma. Circulation 2003; 107(11): 1545–1549.
286. Lam T, Pouliot P, Avti PK, Lesage F, Kakkar AK. Superparamagnetic iron oxide based nanoprobes for imaging and theranostics. Adv Colloid Interface Sci 2013; 199–200: 95–113.
287. Hyafil F, Laissy JP, Mazighi M, Tchetche D, Louedec L, Adle-Biassette H, Chillon S, Henin D, Jacob MP, Letourneur D, Feldman LJ. Ferumoxtran-10-enhanced MRI of the hypercholesterolemic rabbit aorta: relationship between signal loss and macrophage infiltration. Arteriosclerosis Thromb Vasc Biol 2006; 26(1): 176–181.
288. Trivedi RA, JM UK-I, Graves MJ, Kirkpatrick PJ, Gillard JH. Noninvasive imaging of carotid plaque inflammation. Neurology 2004; 63(1): 187–188.
289. Schmitz SA, Taupitz M, Wagner S, Wolf KJ, Beyersdorff D, Hamm B. Magnetic resonance imaging of atherosclerotic plaques using superparamagnetic iron oxide particles. J Magn Reson Imaging 2001; 14(4): 355–361.
290. Trivedi RA, JM UK-I, Graves MJ, Cross JJ, Horsley J, Goddard MJ, Skepper JN, Quartey G, Warburton E, Joubert I, Wang L, Kirkpatrick PJ, Brown J, Gillard JH. In vivo detection of macrophages in human carotid atheroma: temporal dependence of ultrasmall superparamagnetic particles of iron oxide-enhanced MRI. Stroke 2004; 35(7): 1631–1635.
291. Zhang Z, Mascheri N, Dharmakumar R, Li D. Cellular magnetic resonance imaging: potential for use in assessing aspects of cardiovascular disease. Cytotherapy 2008; 10(6): 575–586.
292. Oude Engberink RD, van der Pol SM, Dopp EA, de Vries HE, Blezer EL. Comparison of SPIO and USPIO for in vitro labeling of human

monocytes: MR detection and cell function. Radiology 2007; 243(2): 467–474.
293. Thorek DL, Tsourkas A. Size, charge and concentration dependent uptake of iron oxide particles by non-phagocytic cells. Biomaterials 2008; 29(26): 3583–3590.
294. Raynal I, Prigent P, Peyramaure S, Najid A, Rebuzzi C, Corot C. Macrophage endocytosis of superparamagnetic iron oxide nanoparticles: mechanisms and comparison of ferumoxides and ferumoxtran-10. Invest Radiol 2004; 39(1): 56–63.
295. Herborn CU, Vogt FM, Lauenstein TC, Dirsch O, Corot C, Robert P, Ruehm SG. Magnetic resonance imaging of experimental atherosclerotic plaque: comparison of two ultrasmall superparamagnetic particles of iron oxide. J Magn Reson Imaging 2006; 24(2): 388–393.
296. Tsuchiya K, Nitta N, Sonoda A, Otani H, Takahashi M, Murata K, Shiomi M, Tabata Y, Nohara S. Atherosclerotic imaging using 4 types of superparamagnetic iron oxides: new possibilities for mannan-coated particles. Eur J Radiol 2013; 82(11): 1919–1925.
297. Truijers M, Futterer JJ, Takahashi S, Heesakkers RA, Blankensteijn JD, Barentsz JO. In vivo imaging of the aneurysm wall with MRI and a macrophage-specific contrast agent. Am J Roentgenol 2009; 193(5): W437–441.
298. Richards JM, Shaw CA, Lang NN, Williams MC, Semple SI, MacGillivray TJ, Gray C, Crawford JH, Alam SR, Atkinson AP, Forrest EK, Bienek C, Mills NL, Burdess A, Dhaliwal K, Simpson AJ, Wallace WA, Hill AT, Roddie PH, McKillop G, Connolly TA, Feuerstein GZ, Barclay GR, Turner ML, Newby DE. In vivo mononuclear cell tracking using superparamagnetic particles of iron oxide: feasibility and safety in humans. Circ Cardiovasc Imaging 2012; 5(4): 509–517.
299. Nahrendorf M, Jaffer FA, Kelly KA, Sosnovik DE, Aikawa E, Libby P, Weissleder R. Noninvasive vascular cell adhesion molecule-1 imaging identifies inflammatory activation of cells in atherosclerosis. Circulation 2006; 114(14): 1504–1511.
300. Chacko A-M, Hood ED, Zern BJ, Muzykantov VR. Targeted nanocarriers for imaging and therapy of vascular inflammation. Curr Opinion Colloid Interface Sci 2011; 16(3): 215–227.
301. McAteer MA, Sibson NR, von zur Muhlen C, Schneider JE, Lowe AS, Warrick N, Channon KM, Anthony DC, Choudhury RP. *In vivo* magnetic resonance imaging of acute brain inflammation using microparticles of iron oxide. Nat Med 2007; 13(10): 1253–1258.
302. Hoyte LC, Brooks KJ, Nagel S, Akhtar A, Chen R, Mardiguian S, McAteer MA, Anthony DC, Choudhury RP, Buchan AM. Molecular magnetic resonance imaging of acute vascular cell adhesion molecule-1 expression in a mouse model of cerebral ischemia. J Cereb Blood Flow Metab 2010; 30(6): 1178–1187.
303. Michalska M, Machtoub L, Manthey HD, Bauer E, Herold V, Krohne G, Lykowsky G, Hildenbrand M, Kampf T, Jakob P. Visualization of vascular inflammation in the atherosclerotic mouse by ultrasmall superparamagnetic iron oxide vascular cell adhesion molecule-1-specific nanoparticles. Arteriosclerosis Thromb Vasc Biol 2012; 32(10): 2350–2357.
304. Burtea C, Ballet S, Laurent S, Rousseaux O, Dencausse A, Gonzalez W, Port M, Corot C, Vander Elst L, Muller RN. Development of a magnetic resonance imaging protocol for the characterization of atherosclerotic plaque by using vascular cell adhesion molecule-1 and apoptosis-targeted ultrasmall superparamagnetic iron oxide derivatives. Arteriosclerosis Thromb Vasc Biol 2012; 32(6): e36–e48.
305. Lee SM, Lee SH, Kang HY, Baek SY, Kim SM, Shin MJ. Assessment of musculoskeletal infection in rats to determine usefulness of SPIO-enhanced MRI. Am J Roentgenol 2007; 189(3): 542–548.
306. Gellissen J, Axmann C, Prescher A, Bohndorf K, Lodemann KP. Extra- and intracellular accumulation of ultrasmall superparamagnetic iron oxides (USPIO) in experimentally induced abscesses of the peripheral soft tissues and their effects on magnetic resonance imaging. Magn Reson Imaging 1999; 17(4): 557–567.
307. Kaim AH, Jundt G, Wischer T, O'Reilly T, Frohlich J, von Schulthess GK, Allegrini PR. Functional–morphologic MR imaging with ultrasmall superparamagnetic particles of iron oxide in acute and chronic soft-tissue infection: study in rats. Radiology 2003; 227(1): 169–174.
308. Lee SM, Lee SH, Kang HY, Baek SY, Kim SM, Shin MJ. Assessment of musculoskeletal infection in rats to determine usefulness of SPIO-enhanced MRI. Am J Roentgenology 2007; 189(3): 542–548.
309. Baraki H, Zinne N, Wedekind D, Meier M, Bleich A, Glage S, Hedrich HJ, Kutschka I, Haverich A. Magnetic Resonance Imaging of Soft Tissue Infection with Iron Oxide Labeled Granulocytes in a Rat Model. PLoS ONE 2012; 7(12): e51770; doi: 10.1371/journal.pone.0051770
310. Hoerr V, Tuchscherr L, Huve J, Nippe N, Loser K, Glyvuk N, Tsytsyura Y, Holtkamp M, Sunderkotter C, Karst U, Klingauf J, Peters G, Loffler B, Faber C. Bacteria tracking by *in vivo* magnetic resonance imaging. BMC Biol 2013; 11: 63.
311. Bierry G, Jehl F, Holl N, Sibilia J, Froelich S, Froehlig P, Dietemann JL, Kremer S. Cellular magnetic resonance imaging for the differentiation of infectious and degenerative vertebral disorders: preliminary results. J Magn Reson Imaging 2009; 30(4): 901–906.
312. Ma Y, Pope RM. The role of macrophages in rheumatoid arthritis. Curr Pharm Des 2005; 11(5): 569–580.
313. Simon GH, von Vopelius-Feldt J, Fu Y, Schlegel J, Pinotek G, Wendland MF, Chen MH, Daldrup-Link HE. Ultrasmall supraparamagnetic iron oxide-enhanced magnetic resonance imaging of antigen-induced arthritis: a comparative study between SHU 555 C, ferumoxtran-10, and ferumoxytol. Invest Radiol 2006; 41(1): 45–51.
314. Weissleder R, Stark DD, Engelstad BL, Bacon BR, Compton CC, White DL, Jacobs P, Lewis J. Superparamagnetic iron oxide: pharmacokinetics and toxicity. Am J Roentgenol 1989; 152(1): 167–173.
315. Pouliquen D, Le Jeune JJ, Perdrisot R, Ermias A, Jallet P. Iron oxide nanoparticles for use as an MRI contrast agent: pharmacokinetics and metabolism. Magn Reson Imaging 1991; 9(3): 275–283.
316. Frank JA, Miller BR, Arbab AS, Zywicke HA, Jordan EK, Lewis BK, Bryant LH Jr, Bulte JW. Clinically applicable labeling of mammalian and stem cells by combining superparamagnetic iron oxides and transfection agents. Radiology 2003; 228(2): 480–487.
317. Arbab AS, Bashaw LA, Miller BR, Jordan EK, Lewis BK, Kalish H, Frank JA. Characterization of biophysical and metabolic properties of cells labeled with superparamagnetic iron oxide nanoparticles and transfection agent for cellular MR imaging. Radiology 2003; 229(3): 838–846.
318. Arbab AS, Yocum GT, Wilson LB, Parwana A, Jordan EK, Kalish H, Frank JA. Comparison of transfection agents in forming complexes with ferumoxides, cell labeling efficiency, and cellular viability. Mol Imaging 2004; 3(1): 24–32.
319. Arbab AS, Bashaw LA, Miller BR, Jordan EK, Bulte JW, Frank JA. Intracytoplasmic tagging of cells with ferumoxides and transfection agent for cellular magnetic resonance imaging after cell transplantation: methods and techniques. Transplantation 2003; 76(7): 1123–1130.
320. Bulte JW, Arbab AS, Douglas T, Frank JA. Preparation of magnetically labeled cells for cell tracking by magnetic resonance imaging. Methods Enzymol 2004; 386: 275–299.
321. Frank JA, Zywicke H, Jordan EK, Mitchell J, Lewis BK, Miller B, Bryant LH Jr, Bulte JW. Magnetic intracellular labeling of mammalian cells by combining (FDA-approved) superparamagnetic iron oxide MR contrast agents and commonly used transfection agents. Acad Radiol 2002; 9(2): S484–487.
322. Suzuki Y, Zhang S, Kundu P, Yeung AC, Robbins RC, Yang PC. In vitro comparison of the biological effects of three transfection methods for magnetically labeling mouse embryonic stem cells with ferumoxides. Magn Reson Med 2007; 57(6): 1173–1179.
323. Neri M, Maderna C, Cavazzin C, Deidda-Vigoriti V, Politi LS, Scotti G, Marzola P, Sbarbati A, Vescovi AL, Gritti A. Efficient in vitro labeling of human neural precursor cells with superparamagnetic iron oxide particles: relevance for in vivo cell tracking. Stem Cells 2008; 26(2): 505–516.
324. Montet-Abou K, Montet X, Weissleder R, Josephson L. Transfection agent induced nanoparticle cell loading. Mol Imaging 2005; 4(3): 165–171.
325. Reynolds F, Weissleder R, Josephson L. Protamine as an efficient membrane-translocating peptide. Bioconjugate Chem 2005; 16(5): 1240–1245.
326. Wu YJ, Muldoon LL, Varallyay C, Markwardt S, Jones RE, Neuwelt EA. In vivo leukocyte labeling with intravenous ferumoxides/protamine sulfate complex and in vitro characterization for cellular magnetic resonance imaging. Am J Physiol Cell Physiol 2007; 293(5): 26.
327. Arbab AS, Rad AM, Iskander AS, Jafari-Khouzani K, Brown SL, Churchman JL, Ding G, Jiang Q, Frank JA, Soltanian-Zadeh H, Peck DJ. Magnetically-labeled sensitized splenocytes to identify glioma by MRI: a preliminary study. Magn Reson Med 2007; 58(3): 519–526.
328. Arbab AS, Frank JA. Cellular MRI and its role in stem cell therapy. Regen Med 2008; 3(2): 199–215.
329. Arbab AS, Pandit SD, Anderson SA, Yocum GT, Bur M, Frenkel V, Khuu HM, Read EJ, Frank JA. Magnetic resonance imaging and

confocal microscopy studies of magnetically labeled endothelial progenitor cells trafficking to sites of tumor angiogenesis. Stem Cells 2006; 24(3): 671–678.
330. Bluemke DA, Weber TM, Rubin D, de Lange EE, Semelka R, Redvanly RD, Chezmar J, Outwater E, Carlos R, Saini S, Holland GA, Mammone JF, Brown JJ, Milestone B, Javitt MC, Jacobs P. Hepatic MR imaging with ferumoxides: multicenter study of safety and effectiveness of direct injection protocol. Radiology 2003; 228(2): 457–464.
331. Harisinghani MG, Saini S, Weissleder R, Halpern EF, Schima W, Rubin DL, Stillman AE, Sica GT, Small WC, Hahn PF. Differentiation of liver hemangiomas from metastases and hepatocellular carcinoma at MR imaging enhanced with blood-pool contrast agent Code-7227. Radiology 1997; 202(3): 687–691.
332. Harisinghani MG, Saini S, Weissleder R, Hahn PF, Yantiss RK, Tempany C, Wood BJ, Mueller PR. MR lymphangiography using ultrasmall superparamagnetic iron oxide in patients with primary abdominal and pelvic malignancies: radiographic-pathologic correlation. Am J Roentgenol 1999; 172(5): 1347–1351.
333. Mack MG, Balzer JO, Straub R, Eichler K, Vogl TJ. Superparamagnetic iron oxide-enhanced MR imaging of head and neck lymph nodes. Radiology 2002; 222(1): 239–244.
334. Fleige G, Seeberger F, Laux D, Kresse M, Taupitz M, Pilgrimm H, Zimmer C. In vitro characterization of two different ultrasmall iron oxide particles for magnetic resonance cell tracking. Invest Radiol 2002; 37(9): 482–488.
335. Bulte JW, Douglas T, Witwer B, Zhang SC, Strable E, Lewis BK, Zywicke H, Miller B, van Gelderen P, Moskowitz BM, Duncan ID, Frank JA. Magnetodendrimers allow endosomal magnetic labeling and in vivo tracking of stem cells. Nat Biotechnol 2001; 19(12): 1141–1147.
336. Frank JA, Miller BR, Arbab AS, Zywicke HA, Jordan EK, Lewis BK, Bryant LH, Bulte JWM. Clinically applicable labeling of mammalian and stem cells by combining superparamagnetic iron oxides and transfection agents. Radiology 2003; 228(2): 480–487.
337. Dodd CH, Hsu HC, Chu WJ, Yang P, Zhang HG, Mountz JD Jr, Zinn K, Forder J, Josephson L, Weissleder R, Mountz JM, Mountz JD. Normal T-cell response and in vivo magnetic resonance imaging of T cells loaded with HIV transactivator-peptide-derived superparamagnetic nanoparticles. J Immunol Methods 2001; 256(1/2): 89–105.
338. Ahrens ET, Feili-Hariri M, Xu H, Genove G, Morel PA. Receptor-mediated endocytosis of iron-oxide particles provides efficient labeling of dendritic cells for in vivo MR imaging. Magn Reson Med 2003; 49(6): 1006–1013.
339. Bulte JWM, Zhang S-C, van Gelderen P, Herynek V, Jordan EK, Duncan ID, Frank JA. Neurotransplantation of magnetically labeled oligodendrocyte progenitors: magnetic resonance tracking of cell migration and myelination. Proc Natl Acad Sci U S A 1999; 96(26): 15256–15261.
340. Mahmoudi M, Hosseinkhani H, Hosseinkhani M, Boutry S, Simchi A, Shane Journeay W, Subramani K, Laurent S. Magnetic resonance imaging tracking of stem cells in vivo using iron oxide nanoparticles as a tool for the advancement of clinical regenerative medicine. Chem Rev 2011; 111(2): 253–280.
341. Mizuno H, Tobita M, Uysal AC. Concise review: adipose-derived stem cells as a novel tool for future regenerative medicine. Stem Cells 2012; 30(5): 804–810.
342. Takahashi K, Tanabe K, Ohnuki M, Narita M, Ichisaka T, Tomoda K, Yamanaka S. Induction of pluripotent stem cells from adult human fibroblasts by defined factors. Cell 2007; 131(5): 861–872.
343. Caplan AI. Adult mesenchymal stem cells for tissue engineering versus regenerative medicine. J Cell Physiol 2007; 213(2): 341–347.
344. Lewin JS, Nour SG, Duerk JL. Magnetic resonance image-guided biopsy and aspiration. Top Magn Reson Imaging 2000; 11(3): 173–183.
345. Jing X, Yang L, Duan X, Xie B, Chen W, Li Z, Tan H. In vivo MR imaging tracking of magnetic iron oxide nanoparticle labeled, engineered, autologous bone marrow mesenchymal stem cells following intra-articular injection. Joint Bone Spine 2008; 75(4): 432–438.
346. van Buul GM, Kotek G, Wielopolski PA, Farrell E, Bos PK, Weinans H, Grohnert AU, Jahr H, Verhaar JAN, Krestin GP, van Osch GJVM, Bernsen MR. Clinically translatable cell tracking and quantification by MRI in cartilage repair using superparamagnetic iron oxides. PLoS One 2011; 6(2): e17001; doi: 10.1371/journal.pone.0017001
347. Sharifi S, Bulstra SK, Grijpma DW, Kuijer R. Treatment of the degenerated intervertebral disc; closure, repair and regeneration of the annulus fibrosus. J Tissue Eng Regen Med 2014; doi: 10.1002/term.1866.
348. Jiang X, Chen J, Cai Z, Ya Z, Liu Z, Xie C, Wu Y, Wu P. In vivo tracking superparamagnetic iron oxide labeled adipose derived stem cells to repair rabbit degenerated intervertebral disc. J Clin Rehabil Tissue Eng Res 2011; 15(40): 7515–7519.
349. Lalande C, Miraux S, Derkaoui SM, Mornet S, Bareille R, Fricain JC, Franconi JM, Le Visage C, Letourneur D, Amédée J, Bouzier-Sore AK. Magnetic resonance imaging tracking of human adipose derived stromal cells within three-dimensional scaffolds for bone tissue engineering. Eur Cells Mater 2011; 21: 341–354.
350. Serpooshan V, Zhao M, Metzler SA, Wei K, Shah PB, Wang A, Mahmoudi M, Malkovskiy AV, Rajadas J, Butte MJ. The effect of bioengineered acellular collagen patch on cardiac remodeling and ventricular function post myocardial infarction. Biomaterials 2013; 34(36): 9048–9055.
351. Tallheden T, Nannmark U, Lorentzon M, Rakotonirainy O, Soussi B, Waagstein F, Jeppsson A, Sjögren-Jansson E, Lindahl A, Omerovic E. In vivo MR imaging of magnetically labeled human embryonic stem cells. Life Sci 2006; 79(10): 999–1006.
352. Au KW, Liao SY, Lee YK, Lai WH, Ng KM, Chan YC, Yip MC, Ho CY, Wu EX, Li RA, Siu CW, Tse HF. Effects of iron oxide nanoparticles on cardiac differentiation of embryonic stem cells. Biochem Biophys Res Commun 2009; 379(4): 898–903.
353. Carr CA, Stuckey DJ, Tatton L, Tyler DJ, Hale SJM, Sweeney D, Schneider JE, Martin-Rendon E, Radda GK, Harding SE, Watt SM, Clarke K. Bone marrow-derived stromal cells home to and remain in the infarcted rat heart but fail to improve function: an in vivo cine-MRI study. Am J Physiol Heart Circ Physiol 2008; 295(2): H533–H542.
354. Delo DM, Olson J, Baptista PM, D'Agostino RB Jr, Atala A, Zhu JM, Soker S. Non-invasive longitudinal tracking of human amniotic fluid stem cells in the mouse heart. Stem Cells Dev 2008; 17(6): 1185–1193.
355. Wang L, Deng J, Wang J, Xiang B, Yang T, Gruwel M, Kashour T, Tomanek B, Summer R, Freed D, Jassal DS, Dai G, Glogowski M, Deslauriers R, Arora RC, Tian G. Superparamagnetic iron oxide does not affect the viability and function of adipose-derived stem cells, and superparamagnetic iron oxide-enhanced magnetic resonance imaging identifies viable cells. Magn Reson Imaging 2009; 27(1): 108–119.
356. Vallée JP, Hauwel M, Lepetit-Coiffée M, Bei W, Montet-Abou K, Meda P, Gardier S, Zammaretti P, Kraehenbuehl TP, Herrmann F, Hubbell JA, Jaconi ME. Embryonic stem cell-based cardiopatches improve cardiac function in infarcted rats. Stem Cells Transl Med 2012; 1(3): 248–260.
357. Willenbrock S, Knippenberg S, Meier M, Hass R, Wefstaedt P, Nolte I, Murua Escobar H, Petri S. *In vivo* MRI of intraspinally injected SPIO-labelled human $CD34^+$ cells in a transgenic mouse model of ALS. In Vivo 2012; 26(1): 31–38.
358. Hu SL, Lu PG, Zhang LJ, Li F, Chen Z, Wu N, Meng H, Lin JK, Feng H. In vivo magnetic resonance imaging tracking of SPIO-labeled human umbilical cord mesenchymal stem cells. J Cell Biochem 2012; 113(3): 1005–1012.
359. Jackson JS, Golding JP, Chapon C, Jones WA, Bhakoo KK. Homing of stem cells to sites of inflammatory brain injury after intracerebral and intravenous administration: a longitudinal imaging study. Stem Cell Res Ther 2010; 1(2); doi: 10.1186/scrt17
360. Canzi L, Castellaneta V, Navone S, Nava S, Dossena M, Zucca I, Mennini T, Bigini P, Parati EA. Human skeletal muscle stem cell antiinflammatory activity ameliorates clinical outcome in amyotrophic lateral sclerosis models. Mol Med 2012; 18(1): 401–411.
361. Lu SS, Liu S, Zu QQ, Xu XQ, Yu J, Wang JW, Zhang Y, Shi HB. In vivo MR imaging of intraarterially delivered magnetically labeled mesenchymal stem cells in a canine stroke model. PLoS One 2013; 8(2): e54963; doi: 10.1371/journal.pone.0054963
362. Kallur T, Farr TD, Böhm-Sturm P, Kokaia Z, Hoehn M. Spatio-temporal dynamics, differentiation and viability of human neural stem cells after implantation into neonatal rat brain. Eur J Neurosci 2011; 34(3): 382–393.
363. Ladecola C, Alexander M. Cerebral ischemia and inflammation. Curr Opinion Neurol 2001; 14(1): 89–94.
364. Vezzani A. Inflammation and epilepsy. Epilepsy Curr 2005; 5(1): 1–6.

